Figure 1.

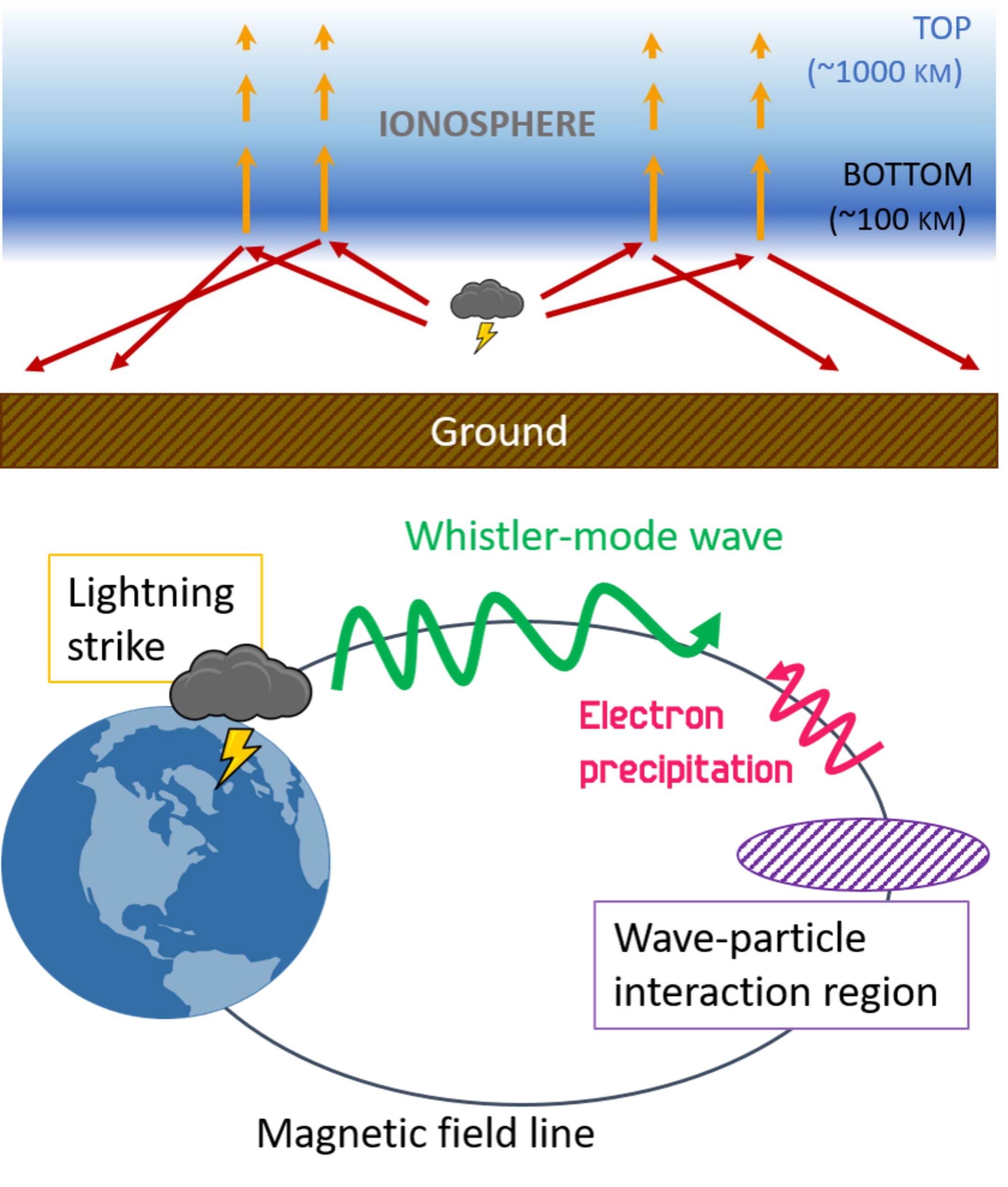

TOP
(~1000 KM)
IONOSPHERE
BOTTOM
(~100 KM)
Ground
Whistler-mode wave
Lightning
strike
Electron
precipitation
Wave-particle
interaction region
Magnetic field line

Figure 2.

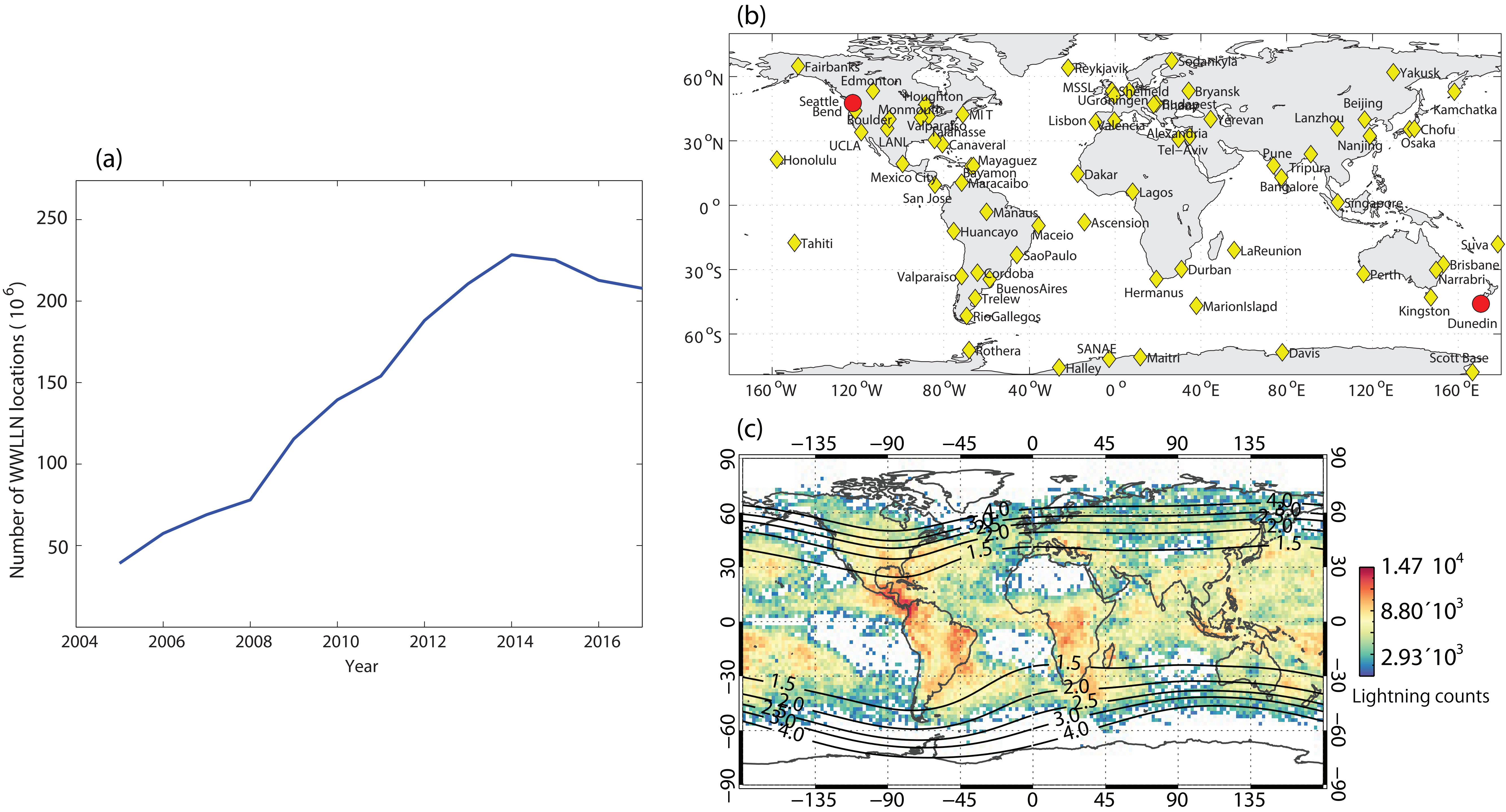

(a)
Number of WWLLN locations (10^6)
Year
(b)
(c)
Lightning counts

Figure 3.

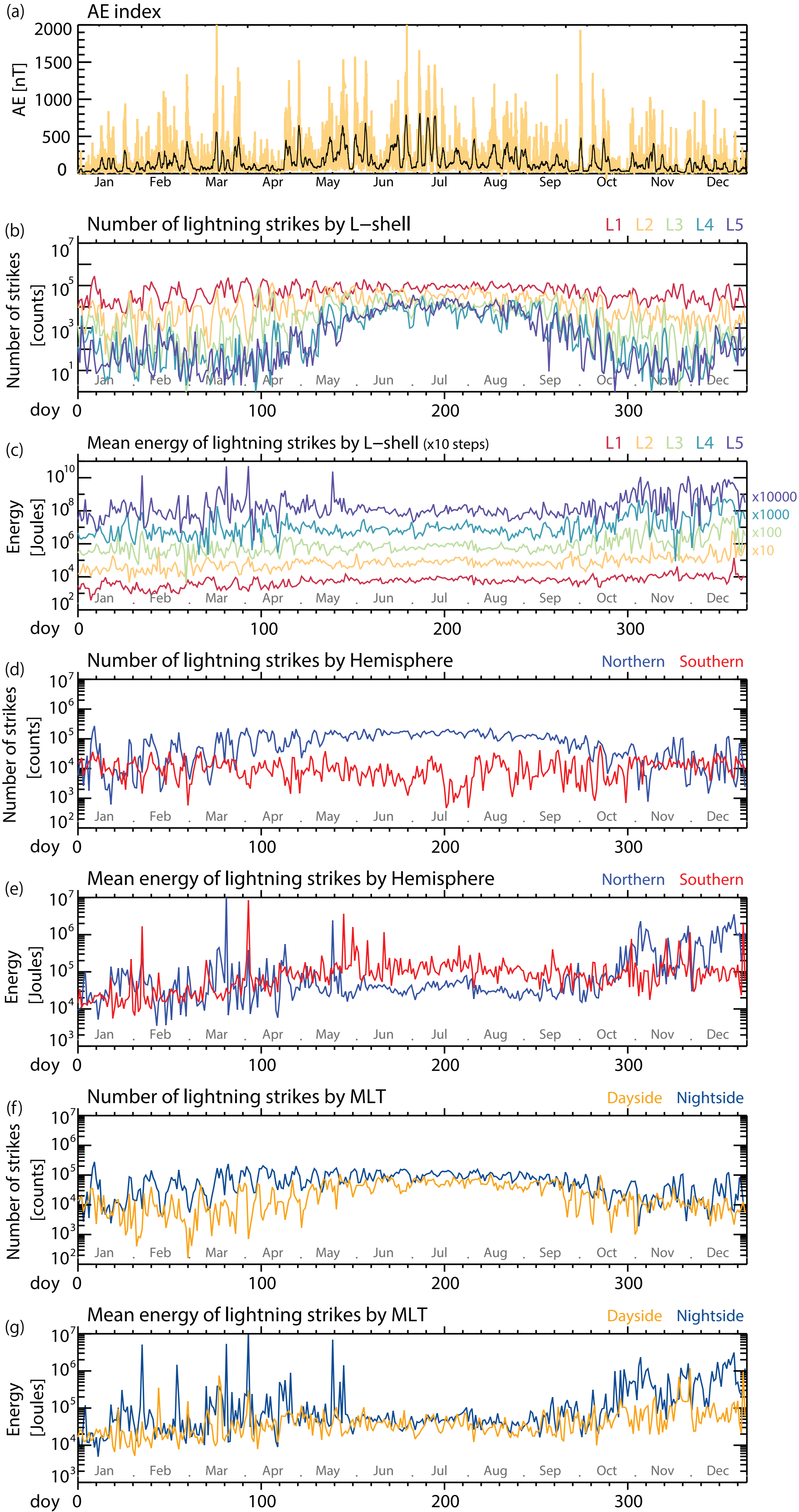
(a) AE index
AE [nT]
2000
1500
1000
500
0
Jan Feb Mar Apr May Jun Jul Aug Sep Oct Nov Dec
(b) Number of lightning strikes by L−shell
L1 L2 L3 L4 L5
Number of strikes [counts]
doy 0 100 200 300
(c) Mean energy of lightning strikes by L−shell (x10 steps)
L1 L2 L3 L4 L5
Energy [Joules]
x10000
x1000
x100
x10
(d) Number of lightning strikes by Hemisphere
Northern Southern
Number of strikes [counts]
(e) Mean energy of lightning strikes by Hemisphere
Northern Southern
Energy [Joules]
(f) Number of lightning strikes by MLT
Dayside Nightside
Number of strikes [counts]
(g) Mean energy of lightning strikes by MLT
Dayside Nightside
Energy [Joules]

Figure 4.

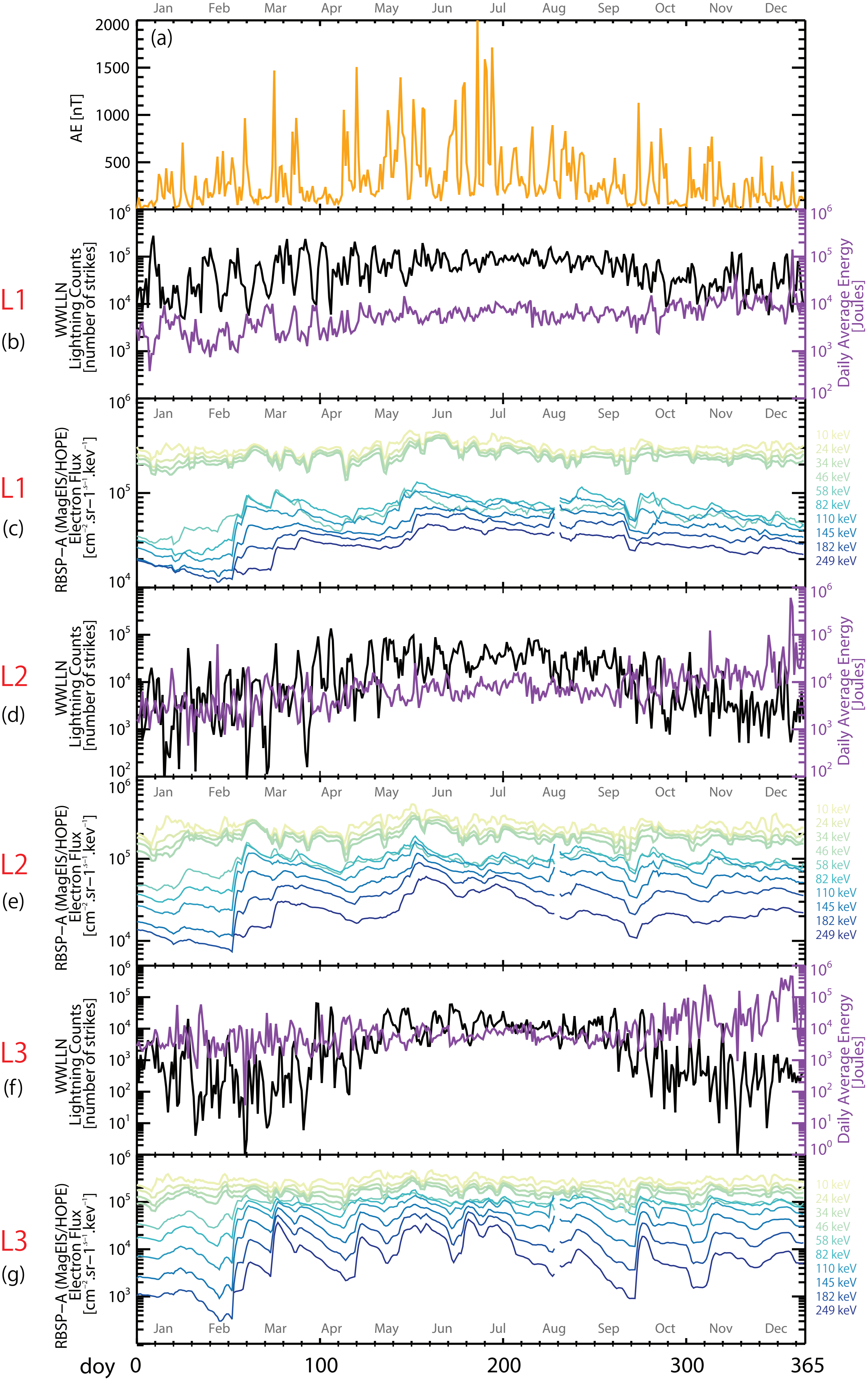

(a)
AE [nT]
2000
1500
1000
500
Jan
Feb
Mar
Apr
May
Jun
Jul
Aug
Sep
Oct
Nov
Dec
L1
(b)
WWLLN
Lightning Counts
[number of strikes]
Daily Average Energy
[Joules]
L1
(c)
RBSP–A (MagEIS/HOPE)
Electron Flux
[cm⁻².sr⁻¹.s⁻¹.keV⁻¹]
10 keV
24 keV
34 keV
46 keV
58 keV
82 keV
110 keV
145 keV
182 keV
249 keV
L2
(d)
L2
(e)
L3
(f)
L3
(g)
doy
0
100
200
300
365

Figure 5.

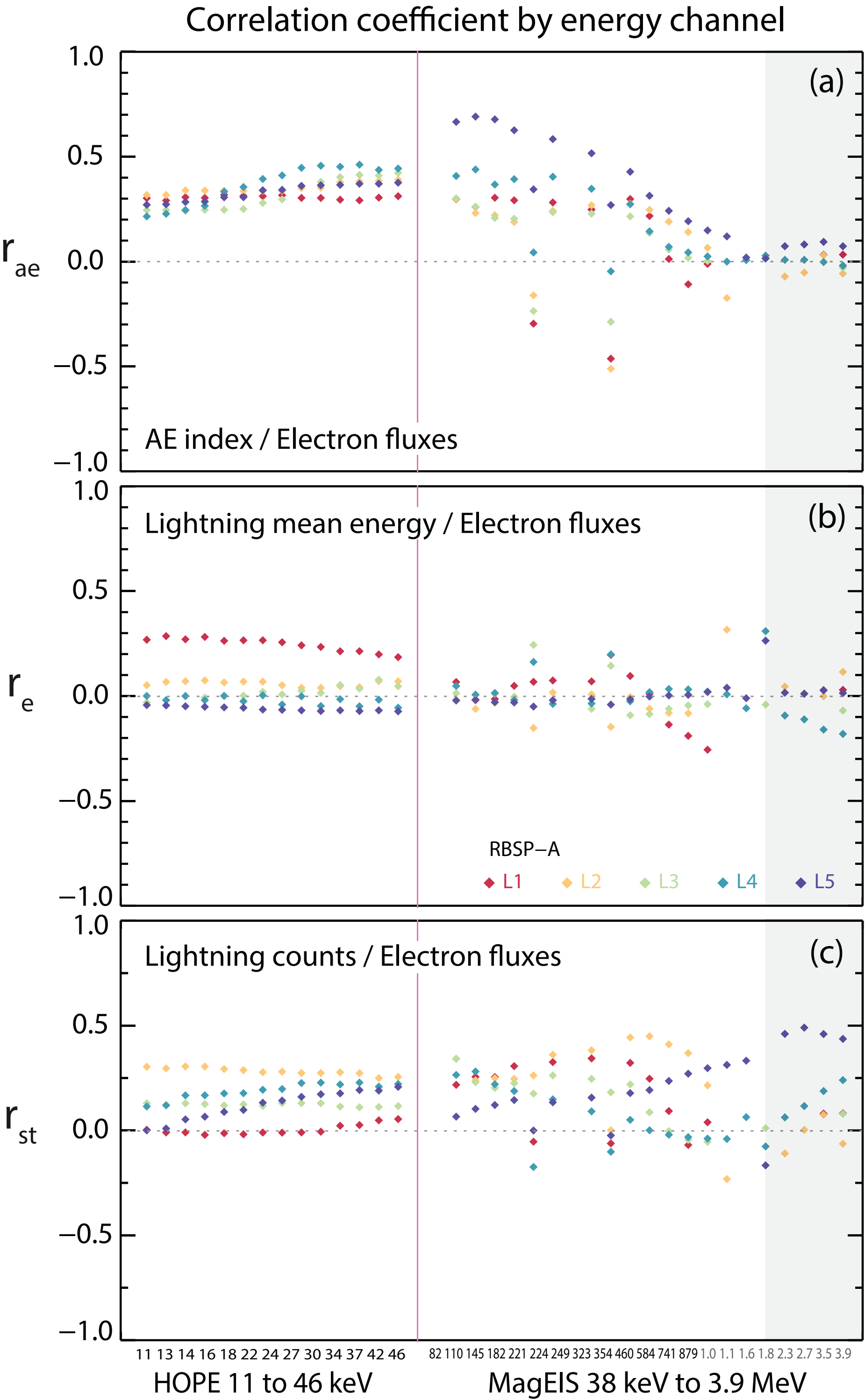

Correlation coefficient by energy channel
(a)
AE index / Electron fluxes
r_{ae}
(b)
Lightning mean energy / Electron fluxes
r_e
RBSP–A
L1
L2
L3
L4
L5
(c)
Lightning counts / Electron fluxes
r_{st}
1.0
0.5
0.0
−0.5
−1.0
11 13 14 16 18 22 24 27 30 34 37 42 46
82 110 145 182 221 224 249 323 354 460 584 741 879 1.0 1.1 1.6 1.8 2.3 2.7 3.5 3.9
HOPE 11 to 46 keV
MagEIS 38 keV to 3.9 MeV

Figure 6.

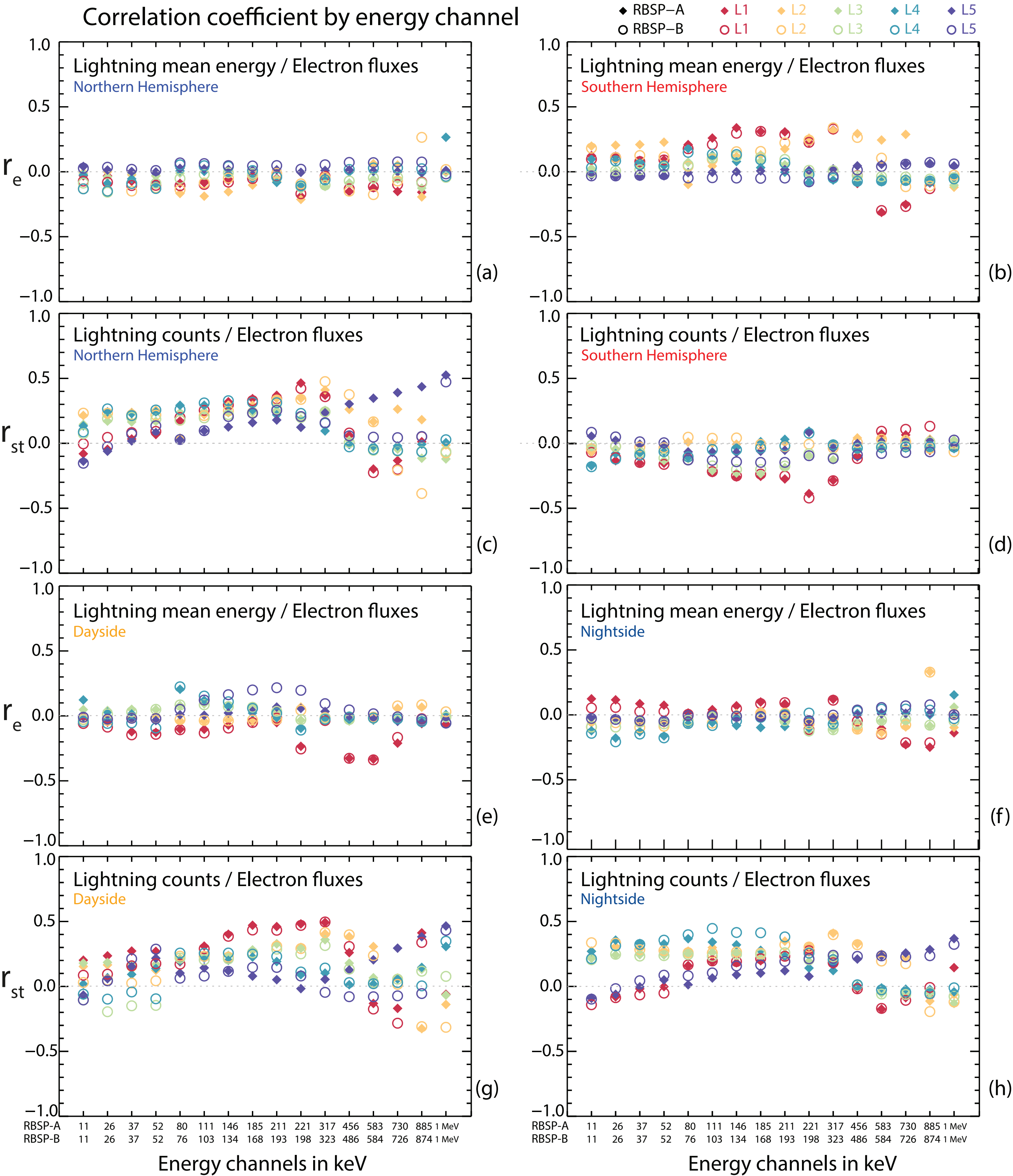

Correlation coefficient by energy channel
RBSP–A
RBSP–B
L1
L2
L3
L4
L5
Lightning mean energy / Electron fluxes
Northern Hemisphere
Southern Hemisphere
Lightning counts / Electron fluxes
Northern Hemisphere
Southern Hemisphere
Lightning mean energy / Electron fluxes
Dayside
Nightside
Lightning counts / Electron fluxes
Dayside
Nightside
r_e
r_{st}
(a)
(b)
(c)
(d)
(e)
(f)
(g)
(h)
RBSP-A 11 26 37 52 80 111 146 185 211 221 317 456 583 730 885 1 MeV
RBSP-B 11 26 37 52 76 103 134 168 193 198 323 486 584 726 874 1 MeV
Energy channels in keV

Figure 7.

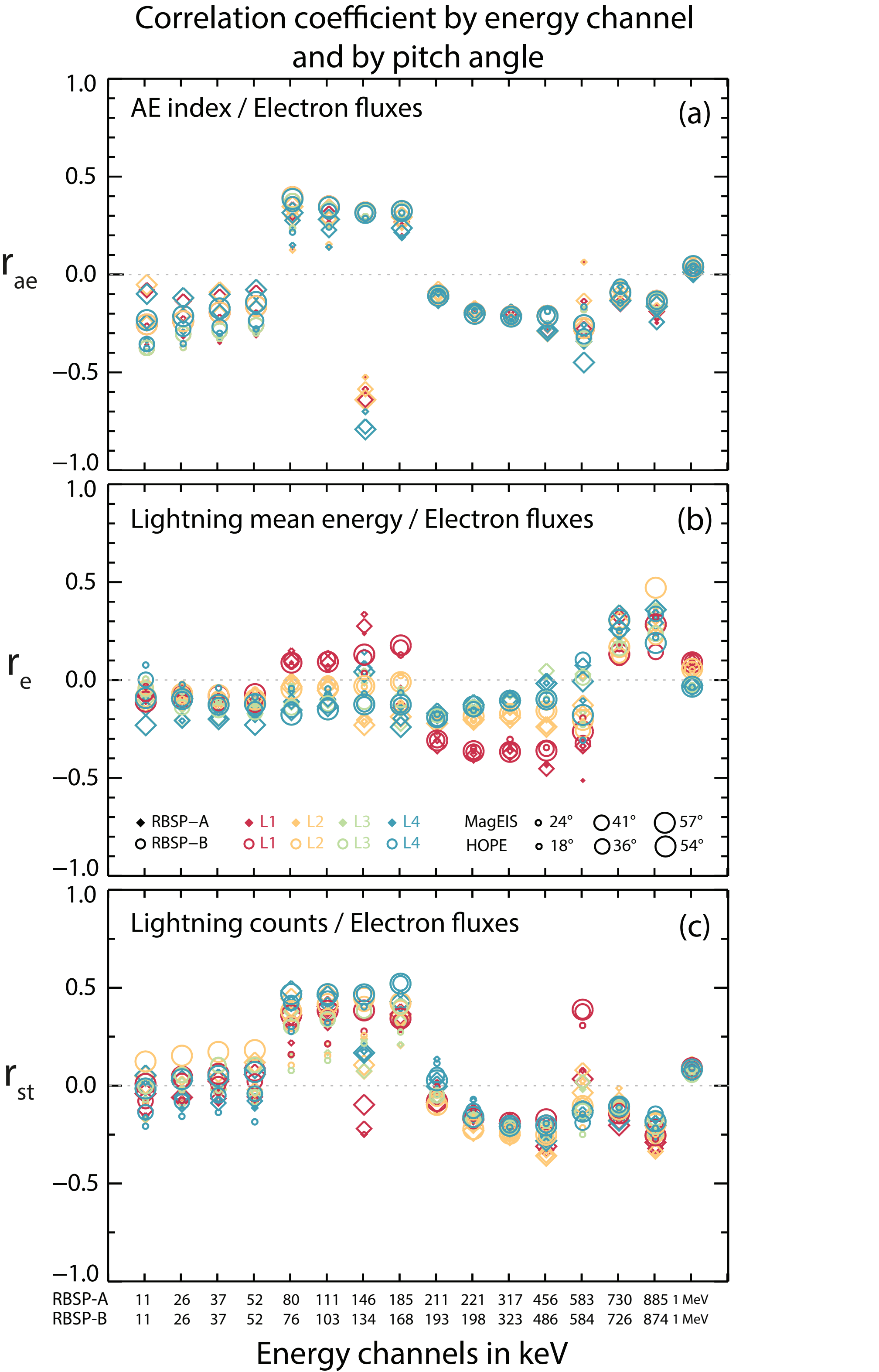

Correlation coefficient by energy channel and by pitch angle
AE index / Electron fluxes
(a)
Lightning mean energy / Electron fluxes
(b)
Lightning counts / Electron fluxes
(c)
r ae
r e
r st
1.0
0.5
0.0
−0.5
−1.0
RBSP−A
RBSP−B
L1 L2 L3 L4
MagEIS 24° 41° 57°
HOPE 18° 36° 54°
RBSP-A 11 26 37 52 80 111 146 185 211 221 317 456 583 730 885 1 MeV
RBSP-B 11 26 37 52 76 103 134 168 193 198 323 486 584 726 874 1 MeV
Energy channels in keV

Figure 8.

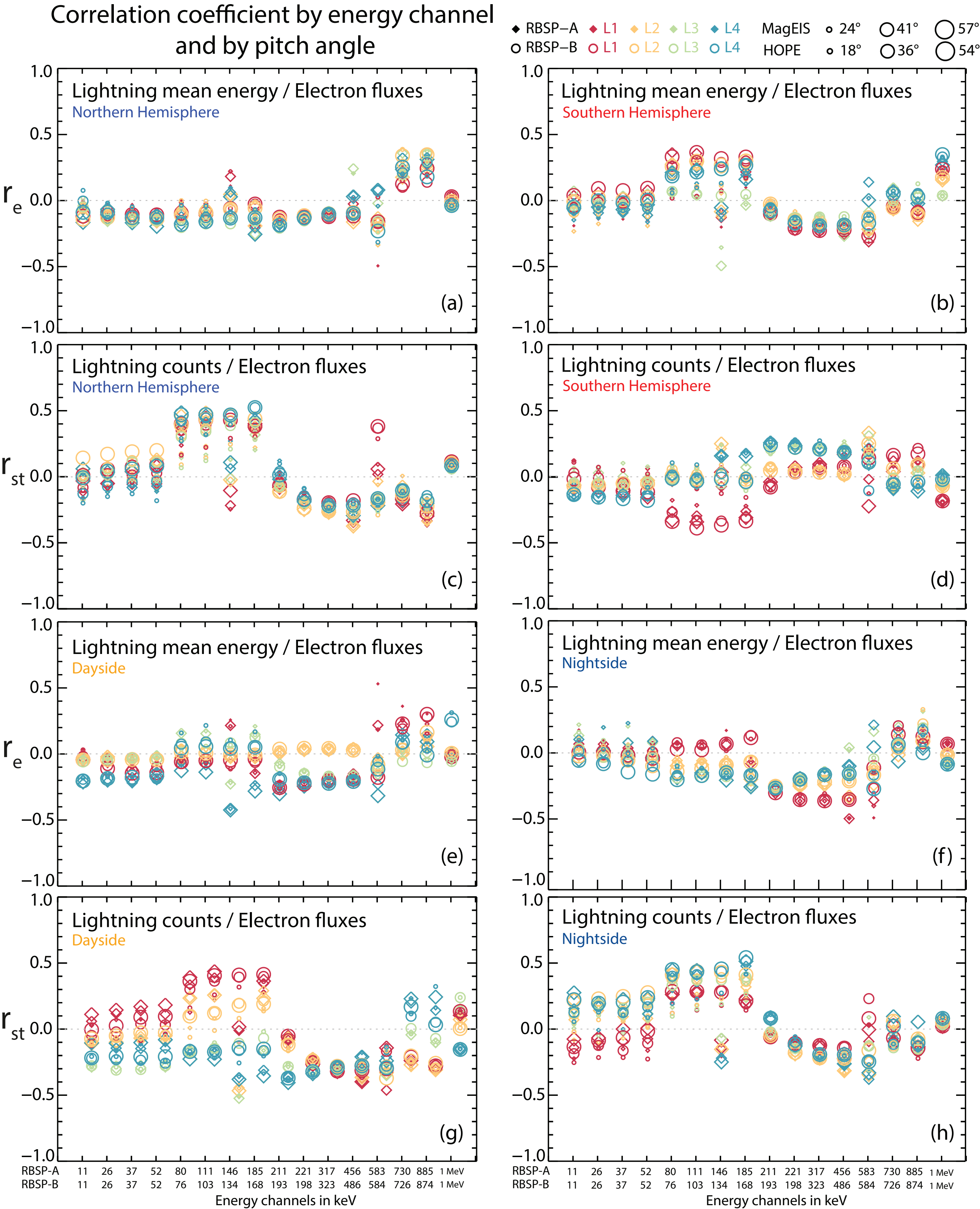
Correlation coefficient by energy channel and by pitch angle
RBSP−A L1 L2 L3 L4
RBSP−B L1 L2 L3 L4
MagEIS 24° 41° 57°
HOPE 18° 36° 54°
Lightning mean energy / Electron fluxes
Northern Hemisphere
(a)
Lightning mean energy / Electron fluxes
Southern Hemisphere
(b)
Lightning counts / Electron fluxes
Northern Hemisphere
(c)
Lightning counts / Electron fluxes
Southern Hemisphere
(d)
Lightning mean energy / Electron fluxes
Dayside
(e)
Lightning mean energy / Electron fluxes
Nightside
(f)
Lightning counts / Electron fluxes
Dayside
(g)
Lightning counts / Electron fluxes
Nightside
(h)
r_e
r_{st}
1.0
0.5
0.0
−0.5
−1.0
RBSP-A 11 26 37 52 80 111 146 185 211 221 317 456 583 730 885 1 MeV
RBSP-B 11 26 37 52 76 103 134 168 193 198 323 486 584 726 874 1 MeV
Energy channels in keV

Figure 9.

		Correlation Results	Theoretical Expectation
4.1 Omnidirectional fluxes	**4.1.1 L-shell**	Low/Moderate Max at E ~ 250 keV for L < 2.5	High for L < 3.5 and E < 1 MeV High for increasing L with decreasing energy
	4.1.2 Hemisphere/MLT	Low/Moderate for L < 2.5 for SH (energy) Higher for NH (counts) Moderate for L < 2.5 (dayside) but no clear MLT dependence.	Higher for NH compared to SH. Higher for the nightside compared to dayside.
	4.1.3 Seasons	Moderate for Autumn for L < 2.5 High for Winter for L > 3.0 (energy) Low for Summer except L < 2.0 at E ~ 200 keV Spring shows highest values, particularly for L > 3.5	Moderate/High for Summer and Low for Winter in NH. Particularly for 100 < E < 350 keV and 2 < L < 3
4.2 Unidirectional fluxes	**4.2.1 L-shell**	No pitch angle dependence, low L dependence Moderate for L < 2.5 and E > 200 keV (energy) Moderate for all L-shells at 80 < E < 185 keV (counts)	High for L < 3.5 at E < 1 MeV Higher correlation for lower pitch angles
	4.2.2 Hemisphere/MLT	Similar to omnidirectional fluxes Generally higher for E ~ 80 - 200 keV and ~41-54 pitch angles Relatively higher correlation for dayside.	Higher for NH compared to SH. Higher for the nightside compared to dayside.
	4.2.3 Seasons	Moderate/High for summer/spring for most L-shells (E ~ 80-317 keV) Higher correlation for L < 3 compared to omnidirectional	Moderate/High for summer and low for winter in NH.

Comparison of long term lightning activity and inner radiation belt electron flux perturbations

C. Martinez-Calderon[1,2], J. Bortnik[2], W. Li[3], H. Spence[4], S. G. Claudepierre[5,2], E. Douma[6] and C. J. Rodger[6]

[1]Institute for Space-Earth Environmental Research, Nagoya University, Nagoya, Japan
[2]Department of Atmospheric and Oceanic Sciences, University of California, Los Angeles, California, USA
[3]Center for Space Physics, Boston University, Boston, Massachusetts, USA
[4]University of New Hampshire, New Hampshire, USA
[5]Space Sciences Department, The Aerospace Corporation, El Segundo, California, USA
[6]University of Otago, Dunedin, New Zealand

Key Points:

- Moderate correlation between lightning activity and electron fluxes on time scales of a few months to a year
- The influence of lightning activity on fluxes, even at low L-shells, is of the same order as that of the AE index
- Seasonal variations, AE index, and MLT influence correlation between lightning activity and trapped electron fluxes

Corresponding author: Claudia Martinez-Calderon, `claudia@isee.nagoya-u.ac.jp`

Abstract

Lightning discharges are known to inject whistler waves into the inner magnetosphere over a wide region around their source. When a discharge occurs, it radiates electromagnetic energy into the Earth-ionosphere waveguide, some of which couples into the whistler-mode and propagates through the ionospheric plasma away from the Earth. Previous studies have discussed the effects of whistler-induced electron precipitation and radiation belt losses associated with lightning. However, to date there has been no research on the long term effects of this accumulated impact. Here, we use data from the World Wide Lightning Location Network (WWLLN), which has continuously monitored global lightning activity since 2004, to obtain one year of lightning data and categorized them into L-shell ranges, hemispheres and magnetic local times. We then use Van Allen Probe's Energetic Particle, Composition, and Thermal Plasma Suite (ECT) from both satellites (RBSP-A/B) to measure particle fluxes in the inner belts under the same criteria. We compare these two quantities by calculating the correlation coefficients between selected electron energy channels, including pitch angle distribution, and lightning activity under different conditions. Although we found a weak to moderate relationship between lightning activity and electron flux perturbations, the correlation was not as strong as expected from theoretical predictions. Variations in electron fluxes related to substorm activity were of the same order of magnitude as that from lightning activity, even at low L-shells.

1 Introduction

During a lightning discharge, broadband Very Low Frequency (VLF, 0.1-10 kHz) wave energy is radiated away from the lightning source (e.g., Rakov & Uman, 2003). As this energy propagates in the Earth-ionosphere waveguide, it can leak into the magnetosphere and couple into the whistler-mode of wave propagation (Figure 1a) (e.g., Bortnik et al., 2006a, 2006b). These lightning-induced whistler-mode waves, typically referred to simply as whistlers, propagate generally unducted in the magnetosphere reaching the geomagnetic equator where they can easily undergo cyclotron resonant interactions with radiation belt electrons (E > 100 keV, Figure 1b). As a result of wave-particle interactions, whistlers change the pitch angle distribution of electrons with energies ranging from a few keV up to ~1 MeV. The pitch angle is defined as the angle between the electron velocity vector and the local magnetic field. Changes in pitch angle lower the reflection point of electrons as they bounce across hemispheres, driving them into the loss cone and causing their precipitation into the upper atmosphere. This phenomenon is commonly known as Lightning-induced Electron Precipitation (LEP) or Whistler-induced electron precipitation (WEP) depending on the sources (e.g., Dungey, 1963; Cornwall, 1964; Tsurutani & Lakhina, 1997; Voss et al., 1998; Bortnik, 2004; Walt, 2005; Gołkowski et al., 2014)

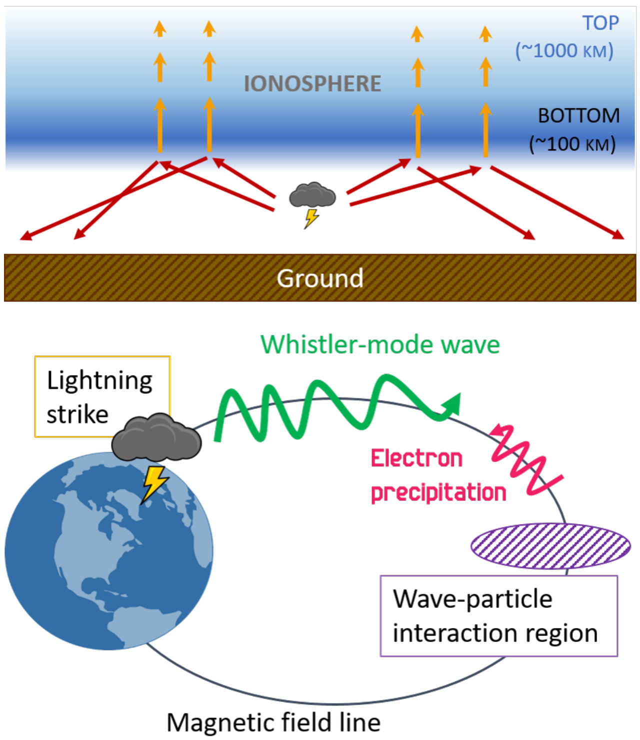

Figure 1. Illustration of VLF energy propagating away from the lightning source, and reaching the geomagnetic equator where it resonantly interacts with electrons.

Even though the effect of whistler-mode waves on electron populations in the radiation belts has been studied extensively (e.g., Meredith et al., 2003; Thorne, 2010; Horne et al., 2005), the main mechanisms behind major losses of electrons remain under discussion. Abel and Thorne (1998a) used quasi-linear Fokker-Plank simulations to study the cumulative long-term effects of wave-particle interactions on scattering and precipitation loss in the inner magnetosphere. For $L > 1.5$ the losses driven by whistler mode waves, including plasmaspheric hiss, lightning-generated whistlers and man-made transmissions, were generally more important than those by Coulomb collisions. The quantitative assessment of these losses accurately reproduced the formation of the slot region. It also predicted that the effect from each loss mechanism was heavily influenced by the characteristics of the wave and the L-shell of interaction. Abel and Thorne (1998b) found that lightning-generated whistlers play a dominant role in the trapped electron population at L > 2, with the largest impact around L=2.4 for 500 keV electrons. The accuracy of this conclusion has been questioned, with Abel and Thorne (1999), opening a debate on both the energy and L-shell range of lightning resonant effects. (Abel & Thorne, 1999) and, later,(Ripoll et al., 2015), while redoing Abel and Thorne [1998a, 1998b, 1999] computations, found slightly different ranges of energy and L-shell. Most effects were for L > 2.5 for energies between 0.1 to 1 MeV and up to L=3.5 for $50 < E < 500$ keV. All these studies confirmed lightning-generated whistlers effects in the slot region (L∼2 – 3.5) for E=0.05 to 1 MeV with energies decreasing with increasing L-shell. They also found these effects to be rather weak, with lifetimes often above ∼ 100 days for these energies (assuming wave amplitude and occurrence rate from Abel and Thorne (1998b)). However it is still difficult to accurately asses the effects of lightning-generated whistlers on radiation belts electrons (i.e., alternative modeling of lightning whistlers properties by Meredith et al. (2007) and Colman and Starks (2013)).

Bortnik et al. (2006b) found that electrons with energies between a few keV up to ∼ 1 MeV can undergo cyclotron resonant interactions with magnetospherically reflected whistlers originating from lightning discharges. This causes enhanced diffusion rates of energetic particles also suggesting that lightning-induced whistlers may play a significant role in the formation of the slot region. Similarly, Blake et al. (2001) show cases where individual thunderstorms were associated with enhanced losses of ∼ 100-200 keV electrons. The extensive amount of precipitation they found suggests that WEP is driven by global thunderstorm activity, and may play an influential role in controlling the lifetimes of electrons in the inner radiation belt.

Additional studies focused on quantifying the trapped electron loss directly related to lightning-induced whistlers. C. J. Rodger et al. (2003) calculated global lightning activity to quantify WEP losses in the radiation belts and their L-shell dependence. Losses by WEP were most significant for 50 to 150 keV electrons for $2.0 < L < 2.4$, and could affect electrons up to ∼225 keV as the L-shell of interaction decreased. Their modeling suggests that WEP due to lightning could be one of the most significant inner radiation belt loss processes for electrons in these particular energy ranges. M. A. Clilverd et al.

(2002) calculated the spatial size of LEP interactions or precipitation patches using Trimpi signatures of subionospheric VLF signals. These are transient perturbations in the amplitude and phase of a received narrowband subionospheric VLF signal. The Trimpi patches were rather large ($\sim$1500 by 600 km), with 38% of the events associated with strong lightning activity. As the electron precipitation is directly related to the size of the precipitation patch, using the values found in their study, they concluded that electron precipitation associated with lightning might be up to 100 times more effective than loss by hiss emissions at L=2.5. More recently, Gołkowski et al. (2014) found that a rough threshold peak current of approximately 100 kA was needed to generate LEP events for the geomagnetic conditions present during their observations. However, previous studies by M. Clilverd et al. (2004) found that observed Trimpi scatter amplitude was produced by precipitation bursts with energy fluxes driven by lightning currents between 70 kA and 250 kA, for smallest and largest detectable fluxes, respectively. These discrepancies can be explained by different signal to noise ratio and open a discussion on the minimum energy necessary to generate LEP events.

Several studies linking lightning generated whistlers to significant electron precipitation, found that the losses depended on the L-shell location and the energy of the electrons interacting with the whistler-mode waves. Others have quantified this loss by using a combination of modeling and observational case studies with one-to-one correspondences during times of high lightning activity. Some of these studies suggest that WEP could be one of the most significant loss processes for these fluxes, implying that these losses should be clearly observable in the variations of trapped electron fluxes. However, the real effect of lightning-related whistlers remain unknown today as it is unclear if these models represent accurately their effect on radiation belt particles. Currently, there are no observational studies focusing on the long term effects of these losses on the trapped electron fluxes of the radiation belts. Thus we conduct, for the first time, a study to determine and quantify the long term effects of lightning-generated whistlers on trapped electron fluxes using particle data from the Van Allen Probes (RBSP) and global lightning distribution.

2 Data and Methods

2.1 WWLLN network

Lightning activity worldwide is monitored using the World Wide Lightning Location Network (WWLLN) (e.g., Lay et al., 2004). WWLLN combines observations from multiple VLF receivers located around the globe to detect, locate, and characterize lightning discharges by detecting lightning generated VLF sferics. Using the "Time of Group Arrival" or TOGA technique (Dowden et al., 2002) observations from each WWLLN station are combined to determine the timing, energy and location of lightning strokes worldwide. VLF sferics from extremely intense lightning discharges can be detected over the entire globe, requiring a minimum of 4 individual TOGA times to produce a valid location on the spherical Earth. In practice, WWLLN requires a minimum of 5 distinct participating station TOGA values to provide a valid lightning location. WWLLN detects signatures of both intra-cloud and cloud-to-ground lightning strokes, without making a distinction between these two types (see the discussion in (C. Rodger et al., 2009)), with a 30% to 50% detection efficiency for strokes above 40 kA. Here we use WWLLN lightning data (version Reloc-B). Currently the WWLLN network has 71 stations that detect VLF radio waves and ∼15–16% of all global cloud-to-ground flashes. The network has been determined to have a temporal accuracy of 15 μ and a spatial accuracy of 10 to 15 km (e.g., C. Rodger et al., 2005; Jacobson et al., 2006). Figure 2a shows how the number of strokes in the Reloc-B dataset varies by year. Figure 2b is a world map showing the locations of the active WWLLN stations in 2014 (yellow diamonds), and the two independent Central Processing Computers (red circles). Note that there are also WWLLN VLF stations at the locations of these processing computers. The primary reason for the variation in the total number of annual WWLLN locations is the number of operational VLF stations. For each lightning stroke, WWLLN data provided the date, time, latitude and longitude, RMS timing error and number of contributing stations that detected the stroke. WWLLN also provides the energy of the radiated stroke in Joules, with the energy error also in Joules, the residual fit error for the location and the number of stations with energy values that were used in the energy number calculations.The technique for determining the lightning power has been described in M. Hutchins et al. (2013).

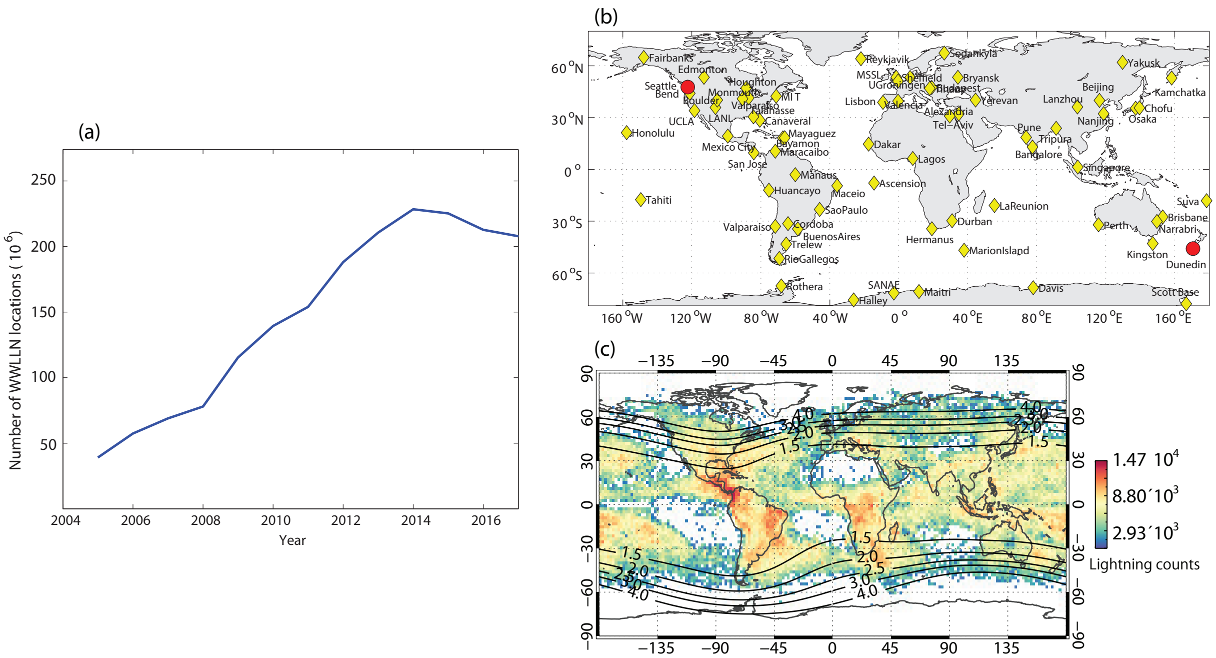

Figure 2. (a) Number of strokes in the Reloc-B dataset as a function of time from 2004 to 2017. (b) Map showing the location of the WWLLN stations as of 2017 (c) Global lightning activity considered in this study in geographic coordinates (including lightning count and energy criteria). Black solid lines indicate the L-shell's footprint using the IGRF model.

2.2 Van Allen Probes data

We use the Energetic Particle, Composition, and Thermal Plasma (ECT) instrument on board RBSP-A and -B to obtain electron fluxes for energies of 30 keV–4 MeV with their respective pitch angle distributions (Spence et al., 2013). Based on previous results by C. J. Rodger et al. (2003) we focus mainly on energy ranges below ∼250 keV, noting however that we also show data up to ∼MeV. For higher energies, we use the Magnetic Electron Ion Spetrometer (MagEIS) instrument which provides unidirectional electron fluxes for the entire energy range (30 keV – 4 MeV) for pitch angles of 8 to 172 degrees. Omnidirectional fluxes are derived from the spin-averaged fluxes (Blake et al., 2001). For lower energies, we use the Helium, Oxygen, Proton, and Electron (HOPE) Mass Spectrometer with energies of 11-52 keV for omnidirectional fluxes, and of 5-52 keV for pitch angles between 4 and 176 degrees (Funsten et al., 2013). To facilitate the comparison we use a simple smoothing to obtain one flux point per day.

Table 1. L-shell categories

Category	L-shell range
L1	$1.5 < L < 2.0$
L2	$2.0 < L < 2.5$
L3	$2.5 < L < 3.0$
L4	$3.0 < L < 3.5$
L5	$L > 3.5$

2.3 Selection Criteria

To discuss long term variation of the trapped electron fluxes in relation to lightning activity and possible seasonal variations we limit this study to a full year. We consider lightning strokes detected by WWLLN from 01 January to 31 December 2013. From Figure 2a, it is clear that the year used in this study is close to the peak for WWLLN detection, with almost 230 million strokes located. To quantify lightning activity, we consider (1) number of lightning strokes (counts) and (2) mean averaged energy detected from these strokes. We note that while WWLLN calculates the global median stroke power seen by the network, the power measured is directly proportional to the peak current providing a realistic return-stroke peak current measurements. The relationship between WWLLN-determined powers and the return-stroke peak currents from individual lightning strokes is presented in detail in M. L. Hutchins et al. (2012).

We can separate our data sets according to two criteria, the first one is to only consider strokes detected by at least 5 contributing stations and with a timing error < 30 ms with their corresponding energy [criteria A]. We can add an energy criteria where we only consider the strokes from criteria A with a relative energy error of $< 70\%$ of the total energy detected [criteria B]. The description on tests of WWLLN energy values has been added as an appendix. Figure 2c shows global lightning activity considered in this study taking into account the two aforementioned criteria. The color gradient indicates the number of lightning strokes detected in a given area. For reference, black solid lines indicate the calculated L-shells projected to the top of the ionosphere with IGRF magnetic field model.

Previous studies found that the role of LEP in comparison to other types of losses is highly dependent on the L-shell of interaction. The large size of electron precipitation patches also suggests that the region of influence might extend beyond the L-shell calculated for the stroke. We consider this by separating the data into 5 L-shell ranges described in Table 1. L-shells were calculated from the latitude and longitude of the detected lightning stroke, projecting it to the geomagnetic equator using two models: IGRF only and IGRF+Tsyganenko 2004 [TS04](Tsyganenko & Sitnov, 2005). For each L-shell range, we obtain the total number of lightning strokes and the corresponding daily mean energy. In order to consider possible energy bias we calculated separate L-shells for criteria A and B defined above. The resulting L-shells were very similar particularly during the summer months in the northern hemisphere, where thunderstorms are more common. The differences between the stroke numbers for criteria A and B increase with increasing L-shell outside of these months. The difference factor usually stays below 4 but can exceptionally reach 25 for $L > 3.5$. These results suggest that at times of high and continuous lightning activity (May-September) the energy measured from the lightning strokes reflects fairly well lightning activity. However, at times when lightning is more variable or reduced (October-April), the confidence in the linkage is reduced. As the results remain fairly similar, for simplicity and to reduce a possibly energy bias, this study will discuss results from criteria A.

We separate the data between northern (latitude $> 0°$) and southern (latitude $< 0°$) hemispheres. For simplicity, all seasons mentioned in the text refer to the northern hemisphere unless stated otherwise. We also separate by Magnetic Local Time (MLT) to consider dayside (06 to 17 MLT) and nightside (18 to 05 MLT) data. Electron flux data from HOPE and MagEIS is categorized in a similar way. Omnidirectional and unidirectional electron fluxes are separated by L ranges and then averaged into daily bins. We define equatorial fluxes as those detected within 15° of the geomagnetic equator. L-shell values from RBSP are provided by HOPE and MagEIS data, respectively, and were calculated with the IGRF+OP77Q model [OP] (Olson & Pfitzer, 1979) which is a good model for the inner magnetosphere. Although the L-shells for WWLLN were calculated using two models, the results from IGRF and TS04 were roughly the same, barring a few days at $L > 3$. Since our study is mostly focused on $L < 4$ and the model used to calculate the L-shells of RBSP data only considers a quiet time magnetosphere, we present the results of this study using the IGRF model only.

3 Lightning activity variability

Figure 3 shows daily lightning activity and mean energy by L-shell range (Figures 3b and 3c), by hemisphere (Figures 3d and 3e) and by MLT (Figures 3f and 3g). In Figures 3b and 3c, L-shell ranges are indicated with colors on the top right, from red to purple (innermost to outermost) following Table 1. For all panels, the horizontal axis shows the day of year (doy) and, for clarity, the corresponding month in gray. We plotted the AE index (Figure 3a, orange) as a function of time with the corresponding daily averaged values (black) used for the correlation calculations further down. We investigate the AE index because substorm activity also contributes to the dynamics of the inner radiation belts by injecting particles into the system. We note no particular correlation between AE and lightning activity, or between AE and the mean energy radiated by lightning strokes.

Lightning activity in Figure 3b shows that during summer time (Jun-Aug), when lightning activity is high, the differences between the number of strokes among the different L-shells is $\sim$2 orders of magnitude. We suppose that at these times lightning is strong and continuous enough to produce significant whistler activity reaching across all L-shells. However, from September to May, lightning activity is more variable showing differences up to $\sim$5 orders of magnitude. In April and November, lightning strokes at L3 are particularly high. For L1, strokes remain almost the same throughout the year. Outside of the summer time, lightning activity remains relatively low at higher L-shells (L4 and L5) . Figure 3c shows the daily mean energy of lightning strokes also separated by L-range. The values corresponding to each L-shell have been artificially multiplied by a factor of 10 for each successive L-range to make it easier to visualize. The variability of the daily mean energy increases with increasing L-shell, in particular for L $>$ 2.5. In agreement with Figure 3b, during the summer the average energy at each L range is fairly similar. At the end of spring and start of autumn, the variations in energy increase with increasing L, particularly in March for L3 to L5. The same ranges show a sharp decrease at the end of November.

Figures 3d and 3e show, respectively, lightning strokes and their mean energies for the northern (blue) and southern (red) hemispheres. We see more clearly that the amount of lightning detected by WWLLN remains fairly constant during the summer time, while it varies of several orders of magnitude over the rest of the year. Lightning activity is

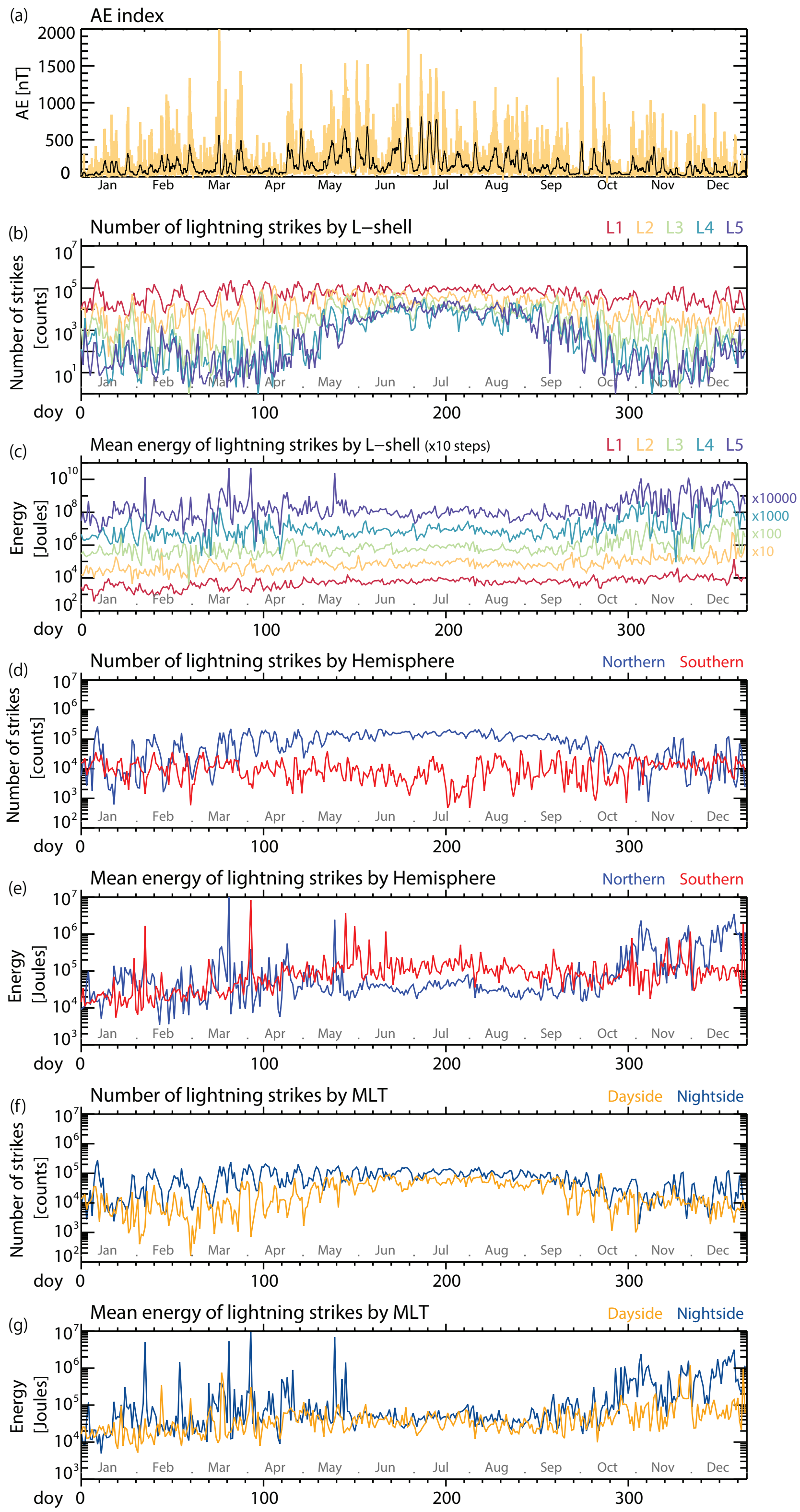

Figure 3. (a) AE index (orange) and 1-day mean average (black). (b) Number of lightning strokes by L-shell, from lowest (red) to highest (blue). (c) Mean energy of lightning strokes by L-shell (x10 each time for ease of observation, multiplier is indicated in the appropriate color to the right of the panel). Number of lightning strokes and their mean energy separated by (d - e) hemisphere and by (f - g) MLT

known to be more common over land masses than over the ocean. As there is more land in the northern hemisphere, more lightning is detected here compared to the southern hemisphere, even when their respective summer periods are compared (Christian et al., 2003). The strokes detected on the southern hemisphere remain highly variable through the year, although from November to March they have similar values to those in the northern hemisphere. From May to September, the mean energy detected in the southern hemisphere is higher than the northern hemisphere. This can be explained by fewer lightning strokes occurring, and detection favoring those with higher energies that are easily detected by the stations. Several peaks of energy lasting a few days reaching up to 10^7 Joules are observed through the year for both hemispheres.

Figure 3f and 3g show lightning activity for the magnetospheric dayside (yellow) and nightside (blue). In summertime, both daily lightning strokes and mean energy are fairly close. Strokes on the dayside fluctuate more than on the nightside (less than 3 orders of magnitude), in particular for February, March and November. The mean energy on the nightside has clear peaks from January to May, with a dip in November which corresponds to a dip observed in energies for L3 to L5 (Figure 3b). This suggests that energy from lightning activity during the nightside MLT reaches higher L-shell values more easily. It is important to note the variations of lightning strokes and mean energy as a function of all these parameters, as it can help us quantify how each of these parameters influences the corresponding variations of electron fluxes.

4 Comparison with electron fluxes

4.1 Omnidirectional electron fluxes

We separated the daily lightning activity, and its corresponding mean energy, by L-range. We compared it to the daily mean averaged fluxes for each energy channel for ECT observations in the corresponding L-shell range. An example of the data for RBSP-A is given in Figure 4 as a function of doy. Figure 4a shows the daily averaged AE index. Figures 4b, 4d and 4f show daily averaged lightning stroke number (black) and mean energy (purple) from L1 to L3. For comparison Figures 4c, 4e and 4g show the averaged daily omnidirectional electron fluxes from RBSP-A for selected energies between 10 and 249 keV (green to purple). For energy ranges on the order of a few hundred keV it is difficult to see any clear relationship between lightning activity and electron fluxes. How-

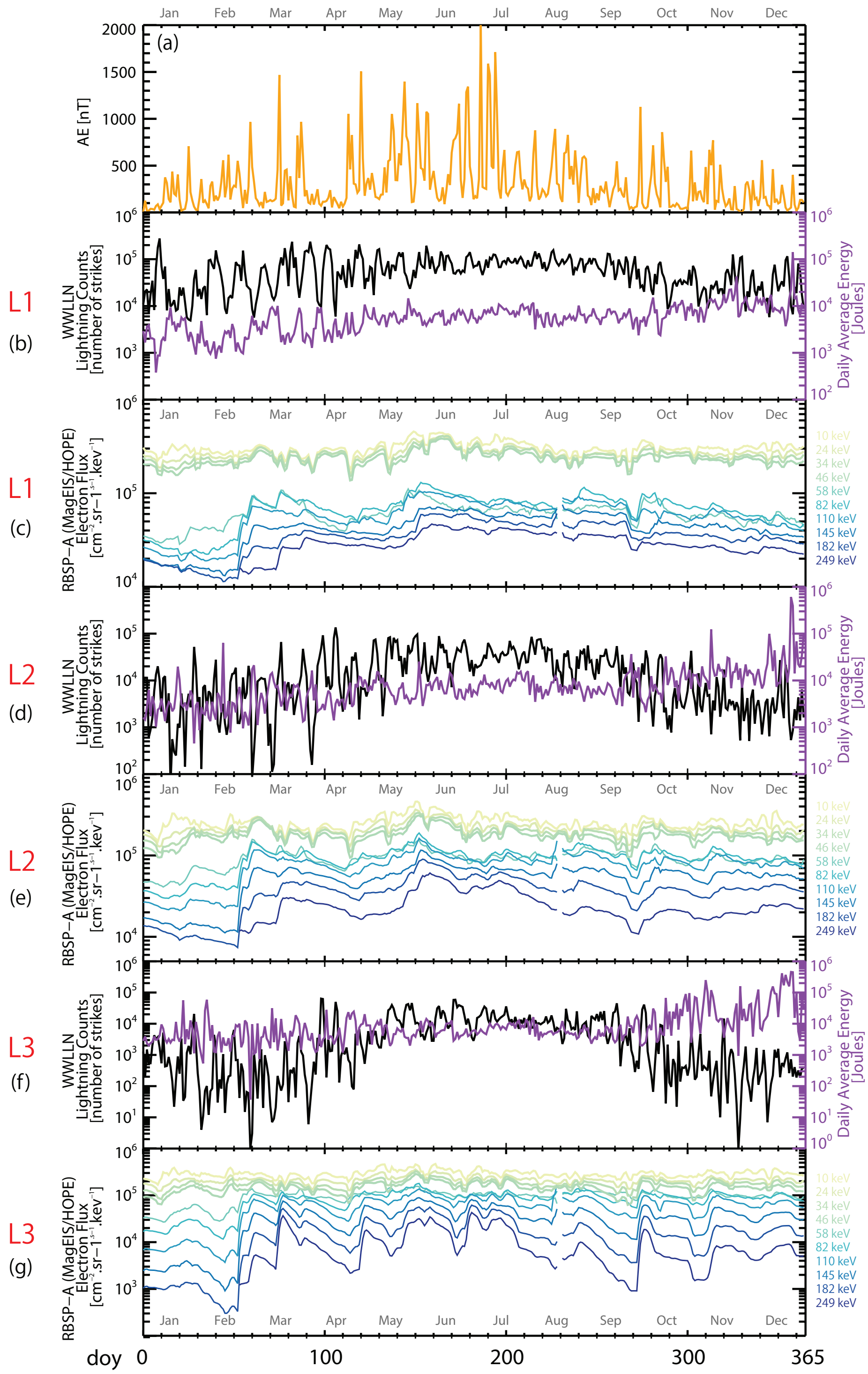

Figure 4. (a) Daily averaged variation of the AE index. Daily averaged lightning counts (black) and averaged daily energy (purple) in Joules for (b) L1, (d) L2 and (f) L3. Averaged electron fluxes from RBSP-A from HOPE (green shades) and MagEIS (blue shades) for selected channels between 10 and 249 keV.

ever, in some cases, increase in lightning number appears to correspond with decrease in fluxes. For example for L1 and L2, the period of sustained lightning activity (June to August) corresponds to a steady decrease of 80 - 211 keV electron fluxes (light blue curves). However, in March to April, a much stronger flux decrease is not associated with lightning activity. To have a better understanding of the long-term relationships between these values, we calculated their correlation coefficients. For each L-shell range, we calculated the linear Pearson correlation coefficient between the energy dependent electron fluxes observed in that L-range and the variation in lightning strokes and mean energy, respectively. The time window for the correlation is one-year and was calculated using the daily-averaged values of all parameters. If the electron fluxes increase or decrease with similar changes in lightning activity, we obtain a positive coefficient, whereas if the fluxes increase while the lightning activity decreases (or vice-versa) we have a negative coefficient. The results of this analysis are described below.

4.1.1 Correlation by L-shell

We calculated the correlation coefficient for each energy channel between 11 keV and 1.6 MeV, for both RBSP-A and RBSP-B, between electron fluxes and lightning activity as a function of different L-shell ranges. While in this figure we show results up to 1.6 MeV, we note however that injections of $\sim$ 700 keV electrons in the inner radiation belts do not occur very often, and thus results at these highest energies should be considered with caution and will be removed from the following figures. Previous studies (e.g., C. J. Rodger et al., 2003; Abel & Thorne, 1998b; Ripoll et al., 2014) suggest that we should focus on energy ranges up to a few MeV for L1 up to hundreds of keV for L3 and above, with most of the interactions expected between 100 to 250 keV for $L <$ 3.0. However, as the energy range is highly dependent upon wave parameters, which might influence the location by $\pm 0.5L$, it is sometimes difficult to know exactly which range to consider. Here we focus on energy ranges between 50 keV and 1 MeV for $L < 3.5$ (L1 to L4). Therefore HOPE data showing the lower energy bins will be particularly helpful at large L values (L4 and L5), while MagEIS data energy bins can be used to find lightning effects over the inner belt and slot region (L1 to L5).

Since the region of wave-particle interactions is generally located near the equator (as the electron gyrofrequency gradient is minimum, (Tsurutani & Smith, 1977; Kennel & Petschek, 1966; Omura & Summers, 2006)), we considered two cases: all fluxes and

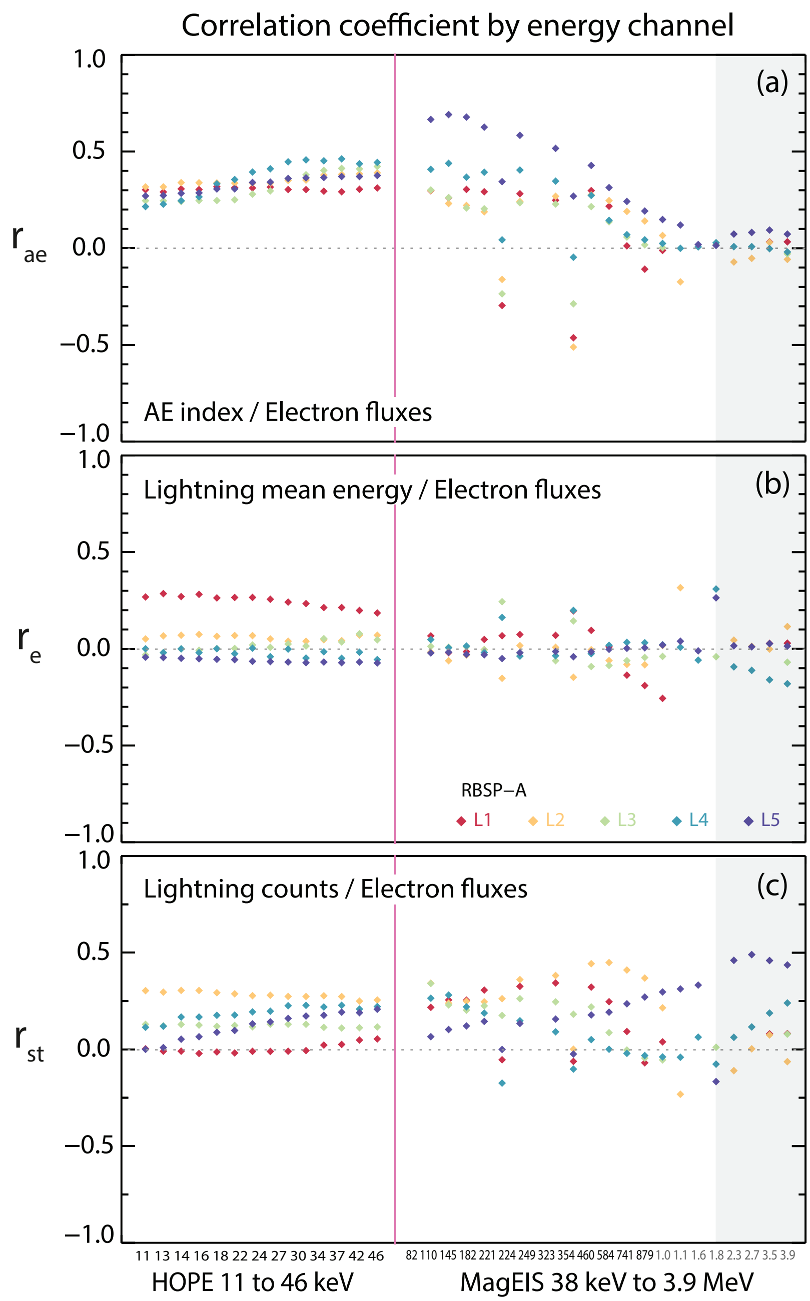

Figure 5. Correlation coefficient magnitude by energy channels between electron fluxes and (a) AE index, (b) Lightning mean energy and (c) number of lightning strokes, respectively. Vertical pink line indicates the change from HOPE to MagEIS values, with increasing energy rightwards. For easier reference, rounded energy channels are indicated at the bottom of the figure. Black indicates energies in keV and gray are in MeV. Gray area in the three panels indicates values above 1.8 MeV

equatorial fluxes only ($|MLAT| < 15°$). As results were similar except for higher variability of non-equatorial fluxes at higher energy ranges, and we focus on long-term relationships for brevity, we will show the results for equatorial fluxes only.

Figure 5 shows an example of the correlation coefficient between RBSP-A electron fluxes and (a) AE index (r_{ae}), (b) lightning mean energy (r_e) and (c) number of lightning strokes (r_{st}) separated by L-shell. Here we show all energy channels available for HOPE (left) and MagEIS (right) for energy ranges of 11-46 keV and 38 keV–3.9 MeV, respectively. Corresponding L-shell ranges are shown in panel (b), with red being the innermost and purple the outermost. For simplicity when discussing energy channels below we will refer to the electron energies from RBSP-A, as the correlation values for RBSP-B are typically very similar. We consider $r < |0.3|$ as no meaningful correlation, $|0.3| < r < |0.7|$ as weak to moderate correlation and $r > |0.7|$ as strong correlation.

Though for most energy channels $r_{ae} < 0.7$, as expected the highest correlation values correspond to the highest L-shells (L $>$ 3.0) (C. J. Rodger et al., 2016; Jaynes et al., 2015). For electrons with energies of $\sim 50-300$keV we have moderate to high positive correlation, suggesting that in the long term, cumulative substorm activity contributes to electron fluxes. Indeed, as substorm activity increases, we expect direct electron injections to contribute to increasing fluxes (Turner et al., 2015). At HOPE energies and above 250 keV the correlation remains low. During active times, whistler-mode waves can be generated due to temperature anisotropy. Substorm injections of electrons also enhance the source populations of these waves. More energy transfers can occur from the electron source population to plasma waves such as chorus or hiss, which in turn accelerate the seed population through wave-particle interactions. We can expect increased electron acceleration at higher energies (Baker et al., 2018; Jaynes et al., 2015), however these conditions might not be significant enough or even visible over longer timescales for $E > 250$ keV. On the other hand this could also reflect a 'lag time' issue, as high energy particles can take up to 2 days to get accelerated; by then a new AE spike might have occurred lowering the correlation. We note also that secondary emissions triggered themselves by lightning-generated whistlers, known as whistler-triggered-chorus (e.g., Nunn & Smith, 1996; Hosseini et al., 2017; Smith & Nunn, 1998) could play a role in the amount of energy that is transferred and also affect the amount of precipitation.

Even though r_e increases to ~ 0.3 for HOPE energies at L1, for most L-shells and electron energies it remains close to zero, suggesting no clear long-term relationship between lightning energy and fluxes. We suggest that only a portion of the WWLLN-detected total energy penetrates the ionosphere and interacts with the particles. Another possibility could be that even if only a portion of energy penetrates, it is unable to exceed a minimum threshold for its influence to be detected over the long term.

At HOPE energies $r_{st} < 0.3$ for all L-shells showing no particular correlation. Similarly, for L3 and L4 the highest values of r_{st} are at E $\sim$ 40 keV suggesting low correlation. For L5, r_{st} steadily increases to a maximum of 0.5 for E $\sim$ 2.6 MeV. More importantly, r_{st} follows a similar trend for L1 and L2 peaking at E $\sim$ 220 keV and $\sim$ 145–220 keV, respectively. Even though the correlation coefficients are not particularly high, they reach a maximum at the energies where C. J. Rodger et al. (2003) found that lightning activity affected precipitation the most for $L < 2.5$. Our results suggest that the number of lightning strokes plays a larger role than the overall radiated energy reported by WWLLN. The correlation maxima for the innermost L-shells show a clear trend suggesting that lightning activity directly influences the variation in the electron fluxes for E $\sim$ 200 keV. At these energies, for L2, r_{st} is only slightly higher than r_{ae} suggesting that the effect of substorm activity and that from lightning are of the same order. However for L1, the difference is more marked indicating that lightning activity may play a more important role. However, the positive correlation shows that fluxes increase with lightning activity which was not the expected outcome. This may be the result of a combined effect with substorm activity. From these general results, it is difficult to conclude or quantify the role lightning activity plays compared to that of the AE index.

4.1.2 Correlation by hemisphere and MLT

Lightning strokes are detected more frequently in the northern hemisphere, however, the mean energy detected by WWLLN is sometimes higher in the southern hemisphere. If there is a significant difference between these variables depending on the hemisphere it should appear in the correlation results. Figure 6 shows the energy-dependent correlation coefficient between either lightning mean energy (a,b,e,f) or strokes (c,d,g,h) and electron fluxes, hemisphere, and MLT. For simplicity, in the following figures we will only consider selected channels rounded up to the nearest keV for RBSP-A (filled diamonds) and RBSP-B (open circles). Figure 6a shows that in the northern hemisphere,

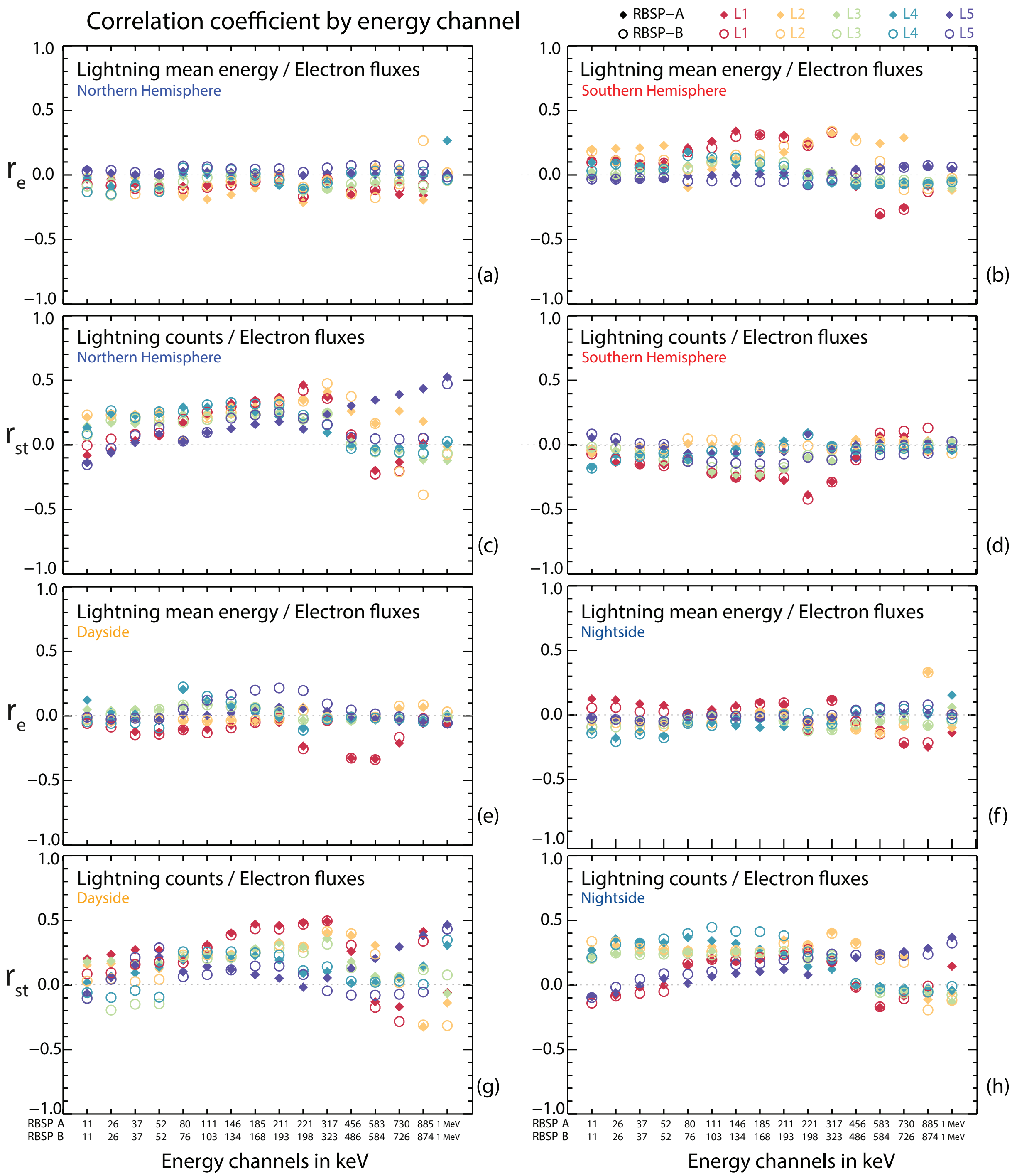

Figure 6. Correlation coefficient by energy channels between electron fluxes and lightning mean energy or lightning strokes, separated by MLT and hemisphere.

r_e remains close to zero in most cases, similarly to Figure 5a. On the other hand, for the southern hemisphere, L1 and L2 show low/moderate positive correlation for electrons with $E \sim 146 - 317$ keV and $317 - 456$ keV, respectively (Figure 6b). These are the energy ranges in which we expect to see the strongest lightning influence. Since lightning energy is overall higher in the southern hemisphere, these results support the idea of an energy threshold: to obtain higher correlations, indicating clear long term influence of lightning activity, there is a certain energy threshold that the lightning strokes must exceed. From numerical simulation on nonlinear wave generation, (Hosseini et al., 2019) found that the upper band chorus was more easily triggered by strong external waves, such as lightning, due to their lower threshold for nonlinear trapping. Since their triggering threshold is much higher, the lower band has a more favorable growth rate, making it harder for the wave to be triggered. Such a mechanism might play a role in the interactions that give birth to lightning-generated whistlers explaining the possible existence of an energy threshold shown of this study.

In the northern hemisphere (Figure 6c), with a higher number of strokes, r_{st} shows comparable results to Figure 5c with a similar maximum for $E \sim 221 - 317$ keV. In the southern hemisphere, r_{st} is close to zero for most cases. We conclude that the correlation observed is mainly due to those strikes in the northern hemisphere, suggesting the existence of a stroke number threshold. There is an exception for L1 at $E = 221$ keV where r_e from southern strokes shows low anti-correlation also seen in Figure 5c, suggesting a different mechanism for these strokes.

As the amount of energy that leaks into the magnetosphere as whistler-mode waves is influenced by the variability of the ionosphere and the magnetosphere, we also separate by night and dayside. Even though the ionosphere becomes far less absorbing to whistler waves, transmitting lightning energy more freely, nightside r_e remains close to zero in most cases (Figure 6f). While comparatively more variable, dayside r_e remains low. We note that for L1, $E \sim 221-583$ keV shows low anti-correlation. This is closer to the behavior expected from quasi-linear theory predictions (Abel & Thorne, 1998a), where greater lightning power corresponds to larger losses and hence lower trapped electron fluxes. However, RBSP takes nearly two years to complete one precession in MLT. In 2013, the spacecraft were spending significantly more time on the nightside than on the dayside, meaning that the 06-12 MLT sector is under sampled. Even though RBSP spent longer time on the nightside, we found no considerable difference for r_e. This shows that the difference between hemispheres plays a more fundamental role than that of MLT when we consider the influence of lightning energy on electron fluxes.

If we consider the number of strokes, night and dayside r_{st} increases with increasing energy channel for L5 reaching 0.5 coherence for $E = 1$ MeV. Dayside r_{st} is only slightly higher suggesting that this effect might be independent on MLT. For these energies at L5, r_{ae} is close to zero suggesting that the variation of fluxes is due to lightning activity. For $L < 3.0$, r_{st} shows mostly no correlation on the nightside, except for $\sim 300{-}400$ keV for L2 and $\sim MeV$ for L3. On the dayside both L1 and L2 show moderate correlation for $E \sim 100 - 400$ keV and $E \sim 300 - 400$ keV, respectively. L3 is the only one that shows moderate correlation for $E < 200$ keV on the nightside. Even though lightning activity for 2013 peaks at approximately 17 MLT, Figure 3f shows that nightside strokes are usually higher than dayside strokes, particularly outside of summer time. This discrepancy can be due to our definition of nightime and the use of MLT. There is a higher number of lightning strokes reaching all L-shell values which can account for the higher correlation at middle L-shell ranges. Even if we take into account MLT, most cases show positive moderate correlation for the L-shells and energies that C. J. Rodger et al. (2003) suggested lightning activity should be more influential. The number of strokes, and not radiated energy, has the strongest empirical link to electron flux variation.

4.1.3 Correlation by seasons

Carpenter and Inan (1987) showed that WEP events have a seasonal dependence, with peaks at the equinoxes due to ionospheric variability. Figure 3d shows that during the summer, lightning activity remains high and stable but is highly variable for the rest of the year. We studied the correlation coefficient considering the seasons defined as one would for the northern hemisphere: Winter: December to February, Spring: March to May, Summer: June to August and Autumn: September to November. For brevity, the figures showing these results are included as supporting information.

Unlike previous cases, the influence of AE index on electron fluxes is seen in all seasons but winter. During summer, $r_{ae} > 3$ for the outermost L-shells (L4, L5) for $E < 221$ keV while the innermost L-shells show no correlation. Summer showed the highest geomagnetic activity, suggesting this is related to substorm injections affecting the outermost L-shells. The highest values of r_e are for winter at L3 and L4 for the energies of interest (50 to 200 keV). Even though the number of strokes can be up to two orders of magnitude lower than during summer (Figure 3), the mean energy from lightning activity for winter is higher at the end of November and December. These results support the previously mentioned hypothesis of an energy threshold in order to see the effects of lightning activity on the long term flux variations.

During summertime, lightning strokes in the northern hemisphere and mean radiated energy for both hemispheres are fairly regular. The cumulative effect of lightning activity should be more evident at these times. However, when we consider lightning activity, r_e and r_{st} show low to no correlation for all L-shells and most energy channels in the summer. The exception being at L1 with moderate negative and positive correlation for $E \sim 100-200$ and $E \sim 300-600$ keV, respectively. Using DEMETER satellite data, Gemelos et al. (2009) found that the drift cone loss electron fluxes had a broad maximum during the northern summer months for the continental United States (and its conjugate region).The DEMETER-observed distribution of the power of VLF waves over the United States also peaked during this time. This indicates precipitation of particles from pitch angle scattering by lightning whistlers in the slot region ($2 < L < 3$). Comparing resonant energy calculated theoretically and assuming corresponding energy peaks from lightning they found correlation values close to 0.42. The largest seasonal differences were at L=2.4 for $E \sim 100-350$ keV which are similar r_e in this study at L1 for E $\sim$ 200 keV. However, in their analysis they only considered nightime data (since the VLF absorption is higher during daytime) and only for the month of August. As our present study did not make distinctions between day and night for seasonal variations, this might explain the discrepancy. They did not consider possible substorm influence either. For the results of this study we suggest that higher substorm activity directly influences the effects of lightning activity on electron fluxes. This could be due to a replenishment of electrons from multiple injections, modifications of the ionospheric and/or magnetospheric conditions making it harder for lightning energy to get through in the whistler-mode or for the whistlers to interact with electrons. At times of high AE index the particles are subject to strong diffusion, their bounce period being larger than the time it takes them to reach the loss cone. This could limit the electrons in the trapped region obfuscating the effect of lightning activity.

Correlation between lightning strikes and fluxes is globally low for summer and winter, but gets higher for autumn and spring at the energies and L-shells of interest, showing a relationship between lightning activity and electron fluxes. In autumn, r_e increases with an increase in lightning energy during October and November. This also correlates with results suggesting that WEP is more important during the equinoxes, probably as a combination of temporally local high lightning activity and favorable propagation conditions for the energy from the lightning strokes. On the other hand, in spring, innermost L-shells show moderate to strong positive correlation even though there is no particular increase of lightning strokes. Even though lightning activity is reduced during spring, the conditions are more favorable for the released energy to interact with trapped electrons, resulting in higher correlation at the L-shells and energies of interest.

In summary, considering several parameters we found two important points: (1) For long term effects of lightning activity to be noticeable, there exists a certain lightning energy threshold. (2) The variations in the AE index play a role on the influence of lightning activity in the fluxes. These two parameters seem to be interlinked and the corresponding influence is difficult to quantify separately. We should consider a way to separate and differentiate the role played by substorm and lightning activity on trapped electron fluxes. We also have to consider the ratio of injection (or acceleration) and loss of particles, as well as the diffusion coefficient controlled by the intensity of the waves interacting with the particles. If the diffusion is slow enough that we are in a case of weak diffusion, the electrons are able to go through several bounce periods before reaching the loss cone. The pitch angle distribution will be independent of the above mentioned factors and only a small portion of particles will be able to go into the loss cone at a given time. We tried to study this in detail by selecting intervals during which we had high lightning counts and energy with low AE ($<$ 100nT) for several days and vice versa. However, we did not find any significant long term meaningful association between lightning counts/energy and electron fluxes. We did not find an automatic decrease of the fluxes at times of low AE and high lightning activity, while periods of high AE with high lightning activity sometimes show flux decreases.

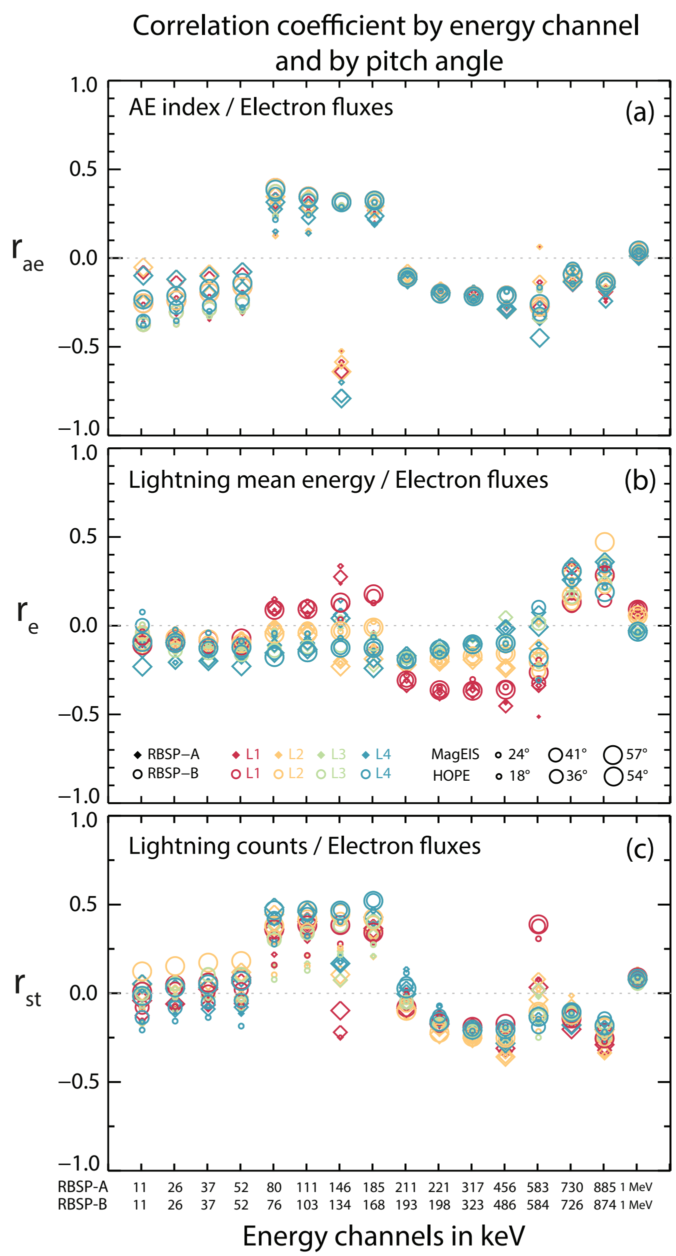

Figure 7. Correlation coefficient magnitude by electron energy channels between electron fluxes and (a) AE index, (b) Lightning mean energy and (c) Lightning strokes as a function of pitch angles. The increasing size of the symbol indicates increasing pitch angles for a given energy between 18° and 57°

4.2 Unidirectional electron fluxes

4.2.1 General results for the pitch angle distribution

If there is some interaction between lightning-generated whistler waves and electrons in the radiation belts, we expect to see an enhancement in the scattering rates of electrons at lower pitch angles rather than higher pitch angles. We calculated the correlation coefficients for each energy channel taking into account the different pitch angles (Figure 7). r_{ae} shows that the correlation values are similar across pitch angles and fairly independent of L-shell. We have moderate positive correlation for $E \sim 70-185$ keV, and low-moderate negative correlation for $E < 52$ keV (Figure 7a). In general, Figure 7b shows that r_e is much higher than previous results. Particularly for L1 at $E \sim$ 185$-$580 keV, showing that when lightning energy increases, electron fluxes at all pitch angles decrease. If we consider lightning strokes in Figure 7c, there is low to no correlation in most cases except for $E \sim$ 80$-$185 keV where we have moderate positive correlation for pitch angles higher than 41°. Although the coefficients remain on the lower side, we see similar tendencies to those of omnidirectional fluxes but with slightly higher coefficients. As expected, at the energies of interest, we see some increase of the fluxes at lower pitch angles with increasing lightning activity, confirming a moderate influence of lightning on long term trapped fluxes.

4.2.2 Correlation by hemisphere and MLT

Figure 8, in a similar format as Figure 6, shows the correlation coefficients for each energy channel as a function of L-shell and pitch angle considering the northern and southern hemispheres separately. In Figures 8a and 8b, r_e shows similar results to Figure 6a and 6b, for both the northern and southern hemispheres, at the electron energies of interest. A comparable result is also found for r_{st} with some differences at $E \sim$ 80$-$200 keV. Figure 8c shows that r_{st} is generally higher for these energies and for pitch angles of $\sim$ 41$-$54°. As the number of lightning strokes is higher in the northern hemisphere, the long term effect of lightning activity is clearer when we consider pitch angle distribution of equatorial electrons.

In Figure 8e, dayside r_e shows some differences compared to omnidirectional fluxes (Figure 6e) showing that higher L-shells reach low-moderate negative correlation at $E \sim$ $146 - 583$ keV. Nightside r_e shown in Figure 8f shows more variability than in Figure

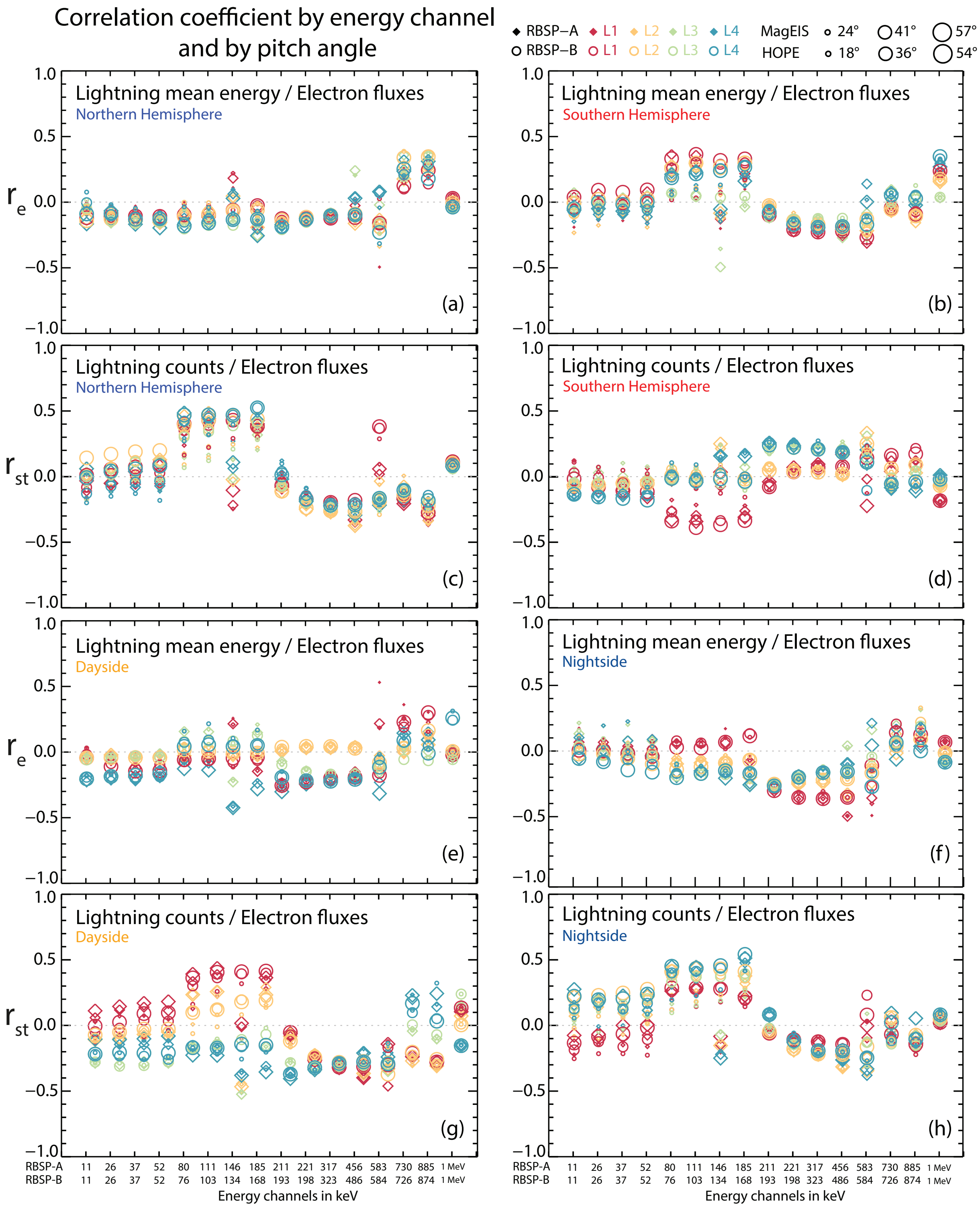

Figure 8. Correlation coefficient calculations separated by electron energy channels between electron fluxes and AE index, lightning mean energy and lightning strokes as a function of pitch angles by hemisphere and MLT. The increasing size of the symbol indicates increasing pitch angles for a given energy between 18° and 57°

6f, reaching moderate negative correlation for L1 and L2 at $E \sim 200 - 730$ keV. Figure 8h shows that nightside r_{st} has the same trends as Figure 6h for omnidirectional fluxes. The main difference is that the correlation coefficients shown here are relatively higher, particularly for the innermost L-shells. The most clear differences between omnidirectional and unidirectional fluxes are observed for dayside r_{st}, Figure 6g and 8g respectively. Here r_{st} is higher for all pitch angles particularly at L1 for $E \sim 80 - 200$ keV with a clear shift to moderate negative correlation at $E \sim 200 - 700$ keV for most L-shells and pitch angles. Figure 8e shows that r_e for the dayside shows differences with Figure 6e depending on the L range, however globally the correlation remains below $|$ 0.3 $|$ for all cases. Nightside results in Figure 8f also show similar results to those of Figure 6f, except for energies between 200 keV and $\sim$ MeV (L1 shows moderate anti-correlations for all pitch angles). Nightside r_{st} shows similar results, with the exception of higher values for $L > L2$ and electron energies between $\sim$ 80 and 200 keV. Dayside r_e shows increased moderate correlations at these energies for L1 and L2. The impact of lightning activity is more clearly seen when we consider pitch angle distribution of the electrons.

4.2.3 Correlation by seasons

We calculated the correlation coefficients considering seasons (Figure not shown for brevity). If we consider r_{ae} for all seasons, contrary to previous results, there is almost no correlation between AE and pitch angle distributions. The influence of substorms activity in low pitch angle distributions is less significant than at higher pitch angles. Since the effect of AE does not seem to be visible in these correlation coefficients, the eventual relationship between lightning activity and pitch angle distributions can be considered as mostly due to lightning activity. In summer time, when global lightning activity is higher, we have moderate to very strong correlation between electrons with $E \sim 80 - 317$ keV and lightning mean energy for most L-shells. r_e reaches a maximum of 0.9 for L1 and L2. Unlike previous results, pitch angles of $\sim 50°$ show strong negative correlation at $E \sim 80{-}211$ keV. On the other hand, r_{st} shows no correlation at lower L-shells but moderate to strong correlation for most pitch angles at L3 and L5. This suggests that, unlike previous results, the average lightning energy has more influence on the increased pitch angle distribution of electrons with energies of a few hundred keV. The relationship between lightning activity and electron fluxes becomes clearer than in any of the previous cases. Similar results are found for the springtime where r_e shows moderate to strong correlations for most pitch angles at the same energy channels as the summer. In spring, r_{st} has moderate positive correlations for L3 and L4. Results for autumn are comparable to those from spring. Finally, during winter, r_e shows moderate correlations with L1 at the same energies as the summer. Similarly, r_{st} shows positive moderate correlations for L2. Generally speaking, we see an increase of the correlation coefficients depending on the pitch angle distributions and for the innermost L-shell ranges. As suggested by Carpenter and Inan (1987), we have higher correlations during the periods including equinoxes. High correlations during the summer time can be explained by the overall increase of global lightning activity during this period.

4.3 Summary and conclusions

The objective of this study was to quantify the long term effects of lightning activity on electron loss in the radiation belts. We used the WWLLN network to measure lightning activity, quantified through the number of strokes and their mean radiated energy, and compared it to variations of the trapped electron fluxes in the inner radiation belt. As previous studies have hinted at the importance of WEP in the variability of the inner belt, their effect should be detectable on long timescales. Using several criteria we have tried to find the relationship that exists between these two values on the time scale of a few days to a year. The results of this study have been summarized in Table 2.

As expected, we found a positive relationship between the AE index and omnidirectional electron fluxes, i.e., as substorm activity increases so do fluxes especially at the outermost L-shells. We also found moderate positive correlation between fluxes and lightning activity, suggesting that electron fluxes increase with increasing lightning activity which was not expected. We note that the eventual effect of lightning activity on electron fluxes is difficult to separate from that of the AE index, and sometimes of the same order of magnitude even at lower L-shells. Although in some cases the correlations between these values are close or below 0.5, a clear trend is seen in most cases suggesting that the effect of lightning activity is still present.

This effect is more clear at the expected energies, globally below $E \sim 200$ keV. The influence varies depending on several criteria, suggesting that the conditions of the ionosphere and magnetosphere in general, and the AE index highly regulate how lightning activity will influence trapped electron fluxes. We found that across a year, the ef-

		Correlation Results	Theoretical Expectation
4.1 Omnidirectional fluxes	**4.1.1 L-shell**	Low/Moderate Max at E ~ 250 keV for L < 2.5	High for L < 3.5 and E < 1 MeV High for increasing L with decreasing energy
	4.1.2 Hemisphere/MLT	Low/Moderate for L < 2.5 for SH (energy) Higher for NH (counts) Moderate for L < 2.5 (dayside) but no clear MLT dependence.	Higher for NH compared to SH. Higher for the nightside compared to dayside.
	4.1.3 Seasons	Moderate for Autumn for L < 2.5 High for Winter for L > 3.0 (energy) Low for Summer except L < 2.0 at E ~ 200 keV Spring shows highest values, particularly for L > 3.5	Moderate/High for Summer and Low for Winter in NH. Particularly for 100 < E < 350 keV and 2 < L < 3
4.2 Unidirectional fluxes	**4.2.1 L-shell**	No pitch angle dependence, low L dependence Moderate for L < 2.5 and E > 200 keV (energy) Moderate for all L-shells at 80 < E < 185 keV (counts)	High for L < 3.5 at E < 1 MeV Higher correlation for lower pitch angles
	4.2.2 Hemisphere/MLT	Similar to omnidirectional fluxes Generally higher for E ~ 80 - 200 keV and ~41-54 pitch angles Relatively higher correlation for dayside.	Higher for NH compared to SH. Higher for the nightside compared to dayside.
	4.2.3 Seasons	Moderate/High for summer/spring for most L-shells (E ~ 80-317 keV) Higher correlation for L < 3 compared to omnidirectional	Moderate/High for summer and low for winter in NH.

Figure 9. Table summarizing the results from this study comparing the correlation results and the corresponding theoretical expectations.

fect of the number of lightning strokes seems more important than that of their average daily energy. However, this can be subject to change depending on the conditions considered. In cases where the mean lightning radiated energy clearly increased while strokes number remained fairly stable, the effect of lightning activity is seen more clearly. Substorm activity plays a role in how lightning impacts upon the fluxes. This result is particularly noticeable when we consider correlation changes as a function of the seasons, in particular for seasons showing moderate to high substorm activity. In cases where substorm activity is not as marked, the effect of lightning is more pronounced suggesting that the variations of electron fluxes are mostly due to lightning activity. However, we are currently unable to definitively quantify and separate the exact role played by either lightning or substorm activity on the long term. At times of higher substorm activity, the correlation between AE and the electron fluxes is of the same order as that from lightning. Further study of the exact effect of each of these parameters should be considered, perhaps using different mathematical techniques.

Since we have one flux point per day, we can also consider that the correlation between lightning and electron fluxes could also be stronger in a more local region. Additionally, the longitudinal asymmetry of the geomagnetic field also plays a role in the amount of particles scattered into the loss cone. Usually, west of the South Atlantic Anomaly in the Americas, electrons are more easily scattered into the loss cone than at European longitudes. We can also point out that the lack of a high correlation for radiated lightning energy could be caused by inaccuracy in the WWLLN-estimated energy. A time lag of a few days is known to exist between substorm enhancements and MeV electron fluxes. Additional cross-correlation analysis to consider this effect has been performed, however because of the length of the current study they will be the subject of a separate paper. Preliminary results show that correlation values increase in most cases for a time lag between 5 to 10 days. We conclude that even though our results demonstrate a relationship between lightning activity and electron fluxes, over the long term this linkage is not as effective as theoretical studies have suggested. Finally, It would be worthwhile to consider doing a similar analysis using other lightning detection networks, such as the UK Met Office ATDnet system or the GLD360 network, as these global networks differ in their characteristics, such as spatial coverage, processing techniques, etc.

Appendix A WWLLN Energy Values Appendix

We have compared the WWLLN (World Wide Lightning Location Network) lightning database to the NZLDN (New Zealand Lightning Detection Network) lightning database in order to test the quality of the WWLLN energy values. We have compared the two networks in the temporal range; 15 April 2009 through to 31 December 2013.

The WWLLN strokes were limited to within 250 km of an NZLDN station, excluding part of the Northern Cape and the South-West Coast of New Zealand (where NZLDN has a reduced detection efficiency). The WWLLN strokes were determined to be the same event as an NZLDN stroke if the temporal difference of the two strokes was $<$ 10 ms and the spatial difference was $<$ 30 km. As NZLDN only detects ground lightning and WWLLN can detect both cloud and ground lightning, we are able to distinguish between the two types of lightning and create data-sets of only ground lightning and only cloud lightning. Lightning strikes observed by both WWLLN and NZLDN make up the ground lightning data-set and those lightning strikes observed solely by WWLLN form the cloud lightning data-set. Overall WWLLN detects 22% of the lightning strikes found by the NZLDN network and under the filtering conditions outlined above this reduces to 19% detection. However, the probability that WWLLN will detect a lightning strike observed by NZLDN increases as the current of the lightning strike increases.

We found the best agreement between the WWLLN energy values and the NZLDN current values when applying the following filter to the WWLLN energy values: 1. At least 3 WWLLN stations must contribute to the energy calculation, and 2. The relative error of the energy value must be $<$ 70%.

Acknowledgments

The authors wish to thank the World Wide Lightning Location Network (http://wwlln.net), a collaboration among over 50 universities and institutions, for providing the lightning location data used in this paper. MagEIS and HOPE data from RBSP can be found at their public database (https://www.rbsp-ect.lanl.gov/science/DataDirectories.php). Solar wind parameters and GOES data are obtained from the OMNI data base via the SPDF/GSFC OMNIWeb (https://omniweb.gsfc.nasa.gov/) This work is supported by the JSPS Program for Advancing Strategic International Networks to Accelerate the Circulation of Talented Researchers under Grant G2602. The research at University of Iowa was supported by JHU/APL contract 921647 under NASA prime contract NAS5-01072. WL would like to acknowledge the NSF grant AGS-1723588 and the Alfred P. Sloan Research Fellowship FG-2018-10936. JB gratefully acknowledges support from NASA LWS grant NNX14AN85G, NASA HTIDeS NNX16AG21G and AFOSR award FA9550-15-1-0158.

References

Abel, B., & Thorne, R. M. (1998a). Electron scattering loss in earth's inner magnetosphere: 1. dominant physical processes. *Journal of Geophysical Research: Space Physics*, *103*(A2), 2385–2396.

Abel, B., & Thorne, R. M. (1998b). Electron scattering loss in earth's inner magnetosphere: 2. sensitivity to model parameters. *Journal of Geophysical Research: Space Physics*, *103*(A2), 2397–2407.

Abel, B., & Thorne, R. M. (1999). Correction to electron scattering loss in the earth's inner magnetosphere: 1, dominant physical processes and electron scattering loss in the earth's inner magnetosphere: 2, sensitivity to model parameters by bob abel and richard m. thorne. *Journal of Geophysical Research: Space Physics*, *104*(A3), 4627–4628.

Baker, D., Erickson, P., Fennell, J., Foster, J., Jaynes, A., & Verronen, P. (2018). Space weather effects in the earths radiation belts. *Space Science Reviews*, *214*(1), 17.

Blake, J., Inan, U., Walt, M., Bell, T., Bortnik, J., Chenette, D., & Christian, H. (2001). Lightning-induced energetic electron flux enhancements in the drift loss cone. *Journal of Geophysical Research: Space Physics*, *106*(A12), 29733–29744.

Bortnik, J. (2004). *Precipitation of radiation belt electrons by lightning-generated magnetospherically reflecting whistler waves* (Unpublished doctoral dissertation). Standford University.

Bortnik, J., Inan, U. S., & Bell, T. F. (2006a). Temporal signatures of radiation belt electron precipitation induced by lightning-generated mr whistler waves: 1. methodology. *Journal of Geophysical Research: Space Physics*, *111*(A2).

Bortnik, J., Inan, U. S., & Bell, T. F. (2006b). Temporal signatures of radiation belt electron precipitation induced by lightning-generated mr whistler waves: 2. global signatures. *Journal of Geophysical Research: Space Physics*, *111*(A2).

Carpenter, D. L., & Inan, U. S. (1987). Seasonal, latitudinal and diurnal distributions of whistler-induced electron precipitation events. *Journal of Geophysical Research: Space Physics*, *92*(A4), 3429–3435.

Christian, H. J., Blakeslee, R. J., Boccippio, D. J., Boeck, W. L., Buechler, D. E., Driscoll, K. T., … others (2003). Global frequency and distribution of lightning as observed from space by the optical transient detector. *Journal of Geophysical Research: Atmospheres*, *108*(D1), ACL–4.

Clilverd, M., Rodger, C., & Nunn, D. (2004). Radiation belt electron precipitation fluxes associated with lightning. *Journal of Geophysical Research: Space Physics*, *109*(A12).

Clilverd, M. A., Nunn, D., Lev-Tov, S. J., Inan, U. S., Dowden, R. L., Rodger, C. J., & Smith, A. J. (2002). Determining the size of lightning-induced electron precipitation patches. *Journal of Geophysical Research: Space Physics*, *107*(A8).

Colman, J., & Starks, M. (2013). Vlf wave intensity in the plasmasphere due to tropospheric lightning. *Journal of Geophysical Research: Space Physics*, *118*(7), 4471–4482.

Cornwall, J. M. (1964). Scattering of energetic trapped electrons by very-low-frequency waves. *Journal of Geophysical Research*, *69*(7), 1251–1258.

Dowden, R. L., Brundell, J. B., & Rodger, C. J. (2002). Vlf lightning location by time of group arrival (toga) at multiple sites. *Journal of Atmospheric and Solar-Terrestrial Physics*, *64*(7), 817–830.

Dungey, J. (1963). Loss of van allen electrons due to whistlers. *Planetary and Space Science*, *11*(6), 591–595.

Funsten, H. O., Skoug, R. M., Guthrie, A. A., MacDonald, E. A., Baldonado, J. R., Harper, R. W., … Chen, J. (2013). Helium, oxygen, proton, and electron (hope) mass spectrometer for the radiation belt storm probes mission. *Space Science Reviews*, *179*(1), 423–484. doi: 10.1007/s11214-013-9968-7

Gemelos, E., Inan, U., Walt, M., Parrot, M., & Sauvaud, J. (2009). Seasonal dependence of energetic electron precipitation: Evidence for a global role of lightning. *Geophysical Research Letters*, *36*(21).

Gołkowski, M., Gross, N., Moore, R., Cotts, B., & Mitchell, M. (2014). Observation of local and conjugate ionospheric perturbations from individual oceanic lightning flashes. *Geophysical Research Letters*, *41*(2), 273–279.

Horne, R. B., Thorne, R. M., Shprits, Y. Y., Meredith, N. P., Glauert, S. A., Smith, A. J., … Decreau, P. M. E. (2005, September). Wave acceleration of electrons in the van allen radiation belts. *Nature*, *437*(7056), 227–230. doi: 10.1038/nature03939

Hosseini, P., Gołkowski, M., & Harid, V. (2019). Remote sensing of radiation belt energetic electrons using lightning triggered upper band chorus. *Geophysical Research Letters*, *46*(1), 37–47.

Hosseini, P., Gołkowski, M., & Turner, D. L. (2017). Unique concurrent observations of whistler mode hiss, chorus, and triggered emissions. *Journal of Geophysical Research: Space Physics*, *122*(6), 6271–6282.

Hutchins, M., Holzworth, R., Virts, K., Wallace, J., & Heckman, S. (2013). Radiated vlf energy differences of land and oceanic lightning. *Geophysical Research Letters*, *40*(10), 2390–2394.

Hutchins, M. L., Holzworth, R. H., Rodger, C. J., & Brundell, J. B. (2012). Far-field power of lightning strokes as measured by the world wide lightning location network. *Journal of Atmospheric and Oceanic technology*, *29*(8), 1102–1110.

Jacobson, A. R., Holzworth, R., Harlin, J., Dowden, R., & Lay, E. (2006). Performance assessment of the world wide lightning location network (wwlln), using the los alamos sferic array (lasa) as ground truth. *Journal of Atmospheric and Oceanic Technology*, *23*(8), 1082–1092.

Jaynes, A., Baker, D., Singer, H., Rodriguez, J., Loto'aniu, T., Ali, A., … others (2015). Source and seed populations for relativistic electrons: Their roles in radiation belt changes. *Journal of Geophysical Research: Space Physics*, *120*(9), 7240–7254.

Kennel, C. F., & Petschek, H. (1966). Limit on stably trapped particle fluxes. *Journal of Geophysical Research*, *71*(1), 1–28.

Lay, E. H., Holzworth, R. H., Rodger, C. J., Thomas, J. N., Pinto, O., & Dowden, R. L. (2004). Wwll global lightning detection system: Regional validation study in brazil. *Geophysical Research Letters*, *31*(3).

Meredith, N. P., Horne, R. B., Glauert, S. A., & Anderson, R. R. (2007). Slot region electron loss timescales due to plasmaspheric hiss and lightning-generated whistlers. *Journal of Geophysical Research: Space Physics*, *112*(A8), n/a–n/a. doi: 10.1029/2007JA012413

Meredith, N. P., Horne, R. B., Thorne, R. M., & Anderson, R. R. (2003). Favored regions for chorus-driven electron acceleration to relativistic energies in the earth's outer radiation belt. *Geophysical Research Letters*, *30*(16), n/a–n/a. doi: 10.1029/2003GL017698

Nunn, D., & Smith, A. (1996). Numerical simulation of whistler-triggered vlf emissions observed in antarctica. *Journal of Geophysical Research: Space Physics*, *101*(A3), 5261–5277.

Olson, W., & Pfitzer, K. (1979). *Magnetospheric magnetic field modeling.* (Tech. Rep.). MCDONNELL DOUGLAS ASTRONAUTICS CO-WEST HUNTINGTON BEACH CALIF.

Omura, Y., & Summers, D. (2006). Dynamics of high-energy electrons interacting with whistler mode chorus emissions in the magnetosphere. *Journal of Geophysical Research: Space Physics*, *111*(A9).

Rakov, V. A., & Uman, M. A. (2003). *Lightning: physics and effects.* Cambridge University Press.

Ripoll, J.-F., Albert, J., & Cunningham, G. (2014). Electron lifetimes from narrowband wave-particle interactions within the plasmasphere. *Journal of Geophysical Research: Space Physics*, *119*(11), 8858–8880.

Ripoll, J.-F., Chen, Y., Fennell, J., & Friedel, R. (2015). On long decays of electrons in the vicinity of the slot region observed by heo3. *Journal of Geophysical Research: Space Physics*, *120*(1), 460–478.

Rodger, C., Brundell, J., & Dowden, R. (2005). Location accuracy of vlf world-wide lightning location (wwll) network: Post-algorithm upgrade. In *Annales geophysicae* (Vol. 23, pp. 277–290).

Rodger, C., Brundell, J., & Holzworth, R. (2009). Improvements in the wwlln network. bigger detection efficiencies through more stations and smarter algorithms.

Rodger, C. J., Clilverd, M. A., & McCormick, R. J. (2003). Significance of lightning-generated whistlers to inner radiation belt electron lifetimes. *Journal of Geophysical Research: Space Physics*, *108*(A12).

Rodger, C. J., Cresswell-Moorcock, K., & Clilverd, M. A. (2016). Nature's grand experiment: Linkage between magnetospheric convection and the radiation belts. *Journal of Geophysical Research: Space Physics*, *121*(1), 171–189.

Smith, A., & Nunn, D. (1998). Numerical simulation of vlf risers, fallers, and hooks observed in antarctica. *Journal of Geophysical Research: Space Physics*, *103*(A4), 6771–6784.

Spence, H. E., Reeves, G., Baker, D., Blake, J., Bolton, M., Bourdarie, S., ... others (2013). Science goals and overview of the radiation belt storm probes (rbsp) energetic particle, composition, and thermal plasma (ect) suite on nasas van allen probes mission. *Space Science Reviews*, *179*(1-4), 311–336.

Thorne, R. M. (2010). Radiation belt dynamics: The importance of wave-particle interactions. *Geophysical Research Letters*, *37*(22), n/a–n/a. doi: 10.1029/2010GL044990

Tsurutani, B. T., & Lakhina, G. S. (1997). Some basic concepts of wave-particle interactions in collisionless plasmas. *Reviews of Geophysics*, *35*(4), 491–501.

Tsurutani, B. T., & Smith, E. J. (1977). Two types of magnetospheric elf chorus and their substorm dependences. *Journal of Geophysical Research*, *82*(32), 5112–5128. doi: 10.1029/JA082i032p05112

Tsyganenko, N., & Sitnov, M. (2005). Modeling the dynamics of the inner magnetosphere during strong geomagnetic storms. *Journal of Geophysical Research: Space Physics*, *110*(A3).

Turner, D., Claudepierre, S., Fennell, J., O'Brien, T., Blake, J., Lemon, C., ... others (2015). Energetic electron injections deep into the inner magnetosphere associated with substorm activity. *Geophysical Research Letters*, *42*(7), 2079–2087.

Voss, H., Walt, M., Imhof, W. L., Mobilia, J., & Inan, U. (1998). Satellite observations of lightning-induced electron precipitation. *Journal of Geophysical Research: Space Physics*, *103*(A6), 11725–11744.

Walt, M. (2005). *Introduction to geomagnetically trapped radiation.* Cambridge University Press.